FACULTY OF BIOSCIENCE ENGINEERING

CELLULAR AUTOMATA FOR SIMULATION OF WATER TRANSPORT IN VARIABLY SATURATED SOIL

word count: 15104

Timon de Nood

Student ID: 01201197

Supervisor(s): Prof. Dr. Ir. Jan Baetens & Prof. Dr. Ir. Wim Cornelis

Master thesis submitted for obtaining the degree: master in Bioscience engineering.

Academic year: 2017 - 2018

GHENT UNIVERSITY

Gent, June 8, 2018

The supervisors, The author,

Prof. Dr. Ir. Jan Baetens Prof. Dr. Ir. Wim Cornelis Timon de Nood

DANKWOORD

Graag wil ik mijn fantastische familie en vrienden bedanken voor de vele steun en toeverlaat tijdens mijn opleiding aan de faculteit alsook tijdens het schrijven van deze thesis.

De totstandkoming van deze thesis is echter geen individuele verwezenlijking, maar het resultaat van een intensieve samenwerking met Jan Baetens. In het bijzonder wil ik hem dan ook graag bedanken voor de samenkomsten, constructieve feedback en zijn talrijke revisies. Mijn dank gaat ook uit naar Wim Cornelis, Aisling Daly, Meisam Rezaei, Jan De Pue en Alfonso Senatore voor hun hulp en vlotte correspondentie.

Als laatste wil ik graag de Universiteit Gent bedanken voor de aanbieding van de opleiding en de interessante vakken die mijn leven enorm verrijkt hebben en me leerden om kritisch en vooruitstrevend na te denken.

SAMENVATTING

Deze masterproef heeft als doel meer inzicht te krijgen in een bestaand model dat water transport in een variabele verzadigde bodem simuleert. Het model zou een mogelijk voordeel kunnen bieden ten opzichte van de gebruikelijke modellen en oplossings methodes van de Richards vergelijking. In eerste instantie wordt het model geïmplementeerd en gecalibreerd in Wolfram Mathematica 11.0.1. Om na te gaan hoe gevoelig het model reageert op het wijzigen van haar parameters wordt vervolgens een globale sensitiviteits analyse uitgevoerd. Daarna wordt aan de hand van een dataset van een veldstudie het model gevalideerd ten opzichte van Hydrus 1D. Finaal wordt een kleine wijziging in het model aangebracht om een probleem op te lossen dat bij de calibratie en validatie tot uiting kwam.

SUMMARY

This thesis aims to gain a better understanding in an existing model that simulates watertransport in a variably saturated soil. This model could offer possible advantages in comparison to the usual models and solving methods of the Richards equation. First, the model is implemented and calibrated in Wolfram Mathematica 11.0.1. Subsequently, to find out how sensitive the model responds to a change it its input parameters, a global sensitivity analysis is performed. The model is then validated to Hydrus 1D using a dataset from a field study. To end, a small model modification is applied to overcome a problem that emerged in the calibration and validation.

CONTENTS

GLOSSARY

A	side surface of one cell
α	inverse of the capillary air entry pressure, ψ_a
β	$\left(\frac{\psi}{\psi_a}\right)^n$
β_0	$\left(\frac{\psi_0}{\psi_a}\right)^n$
C_w	specific retention capacity
h	total hydraulic head
J_w	fluid flux
K_c	hydraulic conductivity
K_r	relative hydraulic conductivity
K_s	saturated hydraulic conductivity
κ	Variance
L	height of the vadose zone (GWT is taken as a reference)
l	fitting parameter related to the tortuosity of the soil (used for the Brooks & Corey- and MVG model)
λ	fitting parameter used for the Brooks & Corey- and MVG model
m = 1-$\frac{1}{n}$	parameter related to the pore-dimension distribution index
N	sample size of the GSA
n	pore-dimension distribution index
P	hydrostatic pressure

ρ	fluid density
q	surface boundary condition, darcy flux
$\hat{S}$	Sobol' indice
S_c	mass source term
S_e	effective saturation
S_s	specific storage, continuity parameter
S_w	water saturation
Δt	time discretization
θ	relative moisture content
θ_r	residual water content
θ_s	saturation water content
θ_{TOT}	total water content
V	volume of one cell
Φ	mass flux
ϕ	porosity
ψ	hydrostatic- or pressure head
ψ_a	capillary air entry pressure
ψ_b	pressure head at the surface boundary
ψ_{min}	condition for a minimal pressure head
ψ_{MIN}	minimal pressure head of the complete pressure head profile
ψ_0	continuity parameter
Δz	spatial discretization
ω	fitting parameter used for the Brooks & Corey- and MVG model

ACRONYMS

CA	Cellular Automation
CFL	Courant–Friedrichs–Lewy (CFL) condition
CML	Coupled-Map Lattice
CPU	Central Processing Unit
FAO	Food and Agriculture Organization
GSA	Global Sensitivity Analysis
GWT	Ground Water Table
HPC	High-Performance Computing
IdE	Integro-Difference Equation
LHS	Latin Hypercube Sampling
MSE	Mean Squared Error
MVG	Mualem- van Genuchten
ODE	Ordinary Differential Equation
PDE	Partial Differential Equation
PdE	Partial Difference equation
SA	Sensitivity Analysis
STM	Spatio-Temporal Model
SWR	Soil Water Retention
SWRC	Soil Water Retention Curve
WRB	World Reference Base

LIST OF FIGURES

LIST OF TABLES

CHAPTER 1

LITERATURE REVIEW

1.1 Introduction

A very important natural process is the hydrological cycle enclosing the movement of water through the environment together with all its interactions (Figure 1.1). It is strongly connected to our everyday life and most living organisms on Earth depend on it. Indeed, 71 percent of the Earth's surface is covered with water (Ahrens, 2000). About 3 percent is considered freshwater, out of which 68 percent is found in glaciers and icecaps and about 30 percent as groundwater. The total amount of water on Earth is fairly constant, but its distribution across the different forms varies and depends on a wide range of climatological variables. Water can move between major different forms by means of physical processes of evaporation, condensation, sublimation, advection, precipitation, percolation, infiltration, surface runoff, and subsurface flow. The sun is the main driver of these, as it heats the surface and thus evaporates water as water vapor into the air. Water vapor rises in open air as a result of buoyancy. However, as altitude increases, air pressure decreases along with the temperature. The lower temperature causes water vapour to condense into liquid water droplets which are heavier than the air, such that these fall down unless supported by a lift force. A high concentration of these droplets becomes visible as a cloud. Most water precipitates back into the oceans or onto land as rain, where water flows across the surface as surface runoff. A portion of this runoff ends up in rivers, with streamflow moving water towards the oceans. Runoff and water emerging from the ground (groundwater) may be stored as freshwater in lakes. Not all runoff flows into rivers, much of the precipitation that reaches the surface infiltrates the soil. Some water infiltrates deep into the ground and replenishes aquifers, which can store freshwater for long periods of time. Some of the infiltrated water stays close to the land surface and can seep back into surface-water bodies as groundwater discharge. Over time, the water returns to the ocean, to continue the water cycle (Ahrens, 2000).

Of particular interest in this thesis is the interaction of the soil with various components of hydrology. *Soil physics* or more broader *environmental soil physics* is the scientific discipline that studies these physical properties and processes occurring within

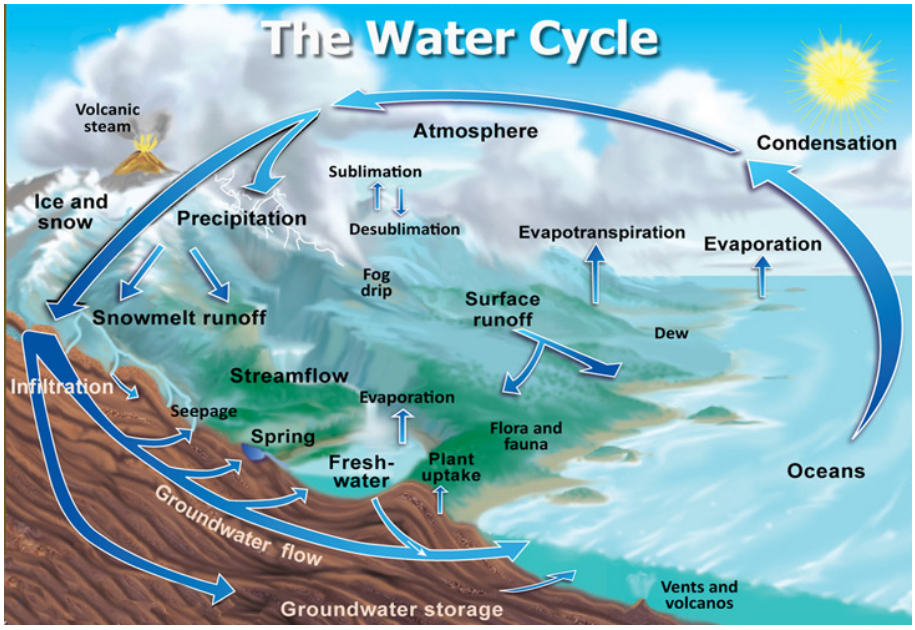

Figure 1.1: Illustration of the water cycle (USGS Water Science School, 2017b).

the vadose zone (Shukla, 2014). The vadose zone is the portion of the soil profile located between the soil-groundwater table (GWT) interface and the atmosphere-soil interface (Figure 1.2). Important soil processes occurring at field to catchment scale include infiltration, drainage, water redistribution, evaporation from the soil, transpiration through plants and deep percolation within the vadose zone. Soil water storage and transport can also be influenced by rainfall, soil types, vegetation and the geology and chemistry of the vadose zone. Soil processes are thus important components of the hydrological cycle and directly influence plant growth and sustenance. It is important to understand all these physical processes, so that one can use these insights to efficiently manage water use. Especially with the growing world population (World Population Clock, 2017), pressure on the land use systems continues to increase (especially on agricultural land). So, in the future, one has to efficiently use water and this is possible only if one understands the soil and the physical phenomena occuring in it (Shukla, 2014).

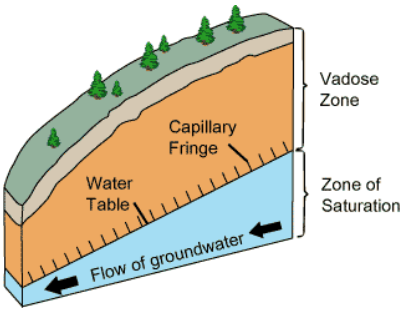

Figure 1.2: Illustration of the vadose zone (USGS Water Science School, 2017a).

The need for an understanding of natural processes has led to the development of different mathematical models. Through mathematical modelling, investigators can often deduce useful information on the subject of study without the need for time-consuming lab or field experiments (Fonstad, 2006). However, there are several critiques to modelling, such as the lack of exactitude from a solely numerical description, the vagueness from the multitude of parameters and the need for computers (Fonstad, 2006). However, these drawbacks do not overshadow the benefits of model-based approaches, such as the computational capacity (i.e. simulation in very small to very large space-time scales) or the possibility to answer ”what if?” questions (i.e. direct observations and predictions of system dynamics) (Nopens, 2015).

The fields of hydrology and related processes, more specifically soil physics, are no exceptions to this. To mathematically describe soil water flow there are several equations, such as the Darcy equation that describes saturated fluid flow (Darcy, 1856). However, this dissertation covers unsaturated fluid flow in the vadose zone where the pores of the soil are not completely filled with water. The equation for describing this kind of flow is a more complex partial differential equation, the so called Richards equation (Richardson, 1922; Richards, 1931), which is derived from the modified Buckingham-Darcy flux equation (Buckingham, 1907) combined with a continuity equation. There are, however, alternative approaches, in adition to the Richards equation, to describe soil water flow and some of these will be discussed in the subsequent sections, together with their (dis)advantages.

1.2 Modelling of Unsaturated Flow

This section outlines how unsaturated flow can be modelled. Firstly, the Richards equation will be derived and the limitations of this equation will be indicated. Then, an overview of alternative spatio-temporal models will be given to conclude with the outline of one of these to describe unsaturated soil waterflow.

1.2.1 The Richards Equation

The Richards equation is constructed from the Buckingham-Darcy flux law (Buckingham, 1907) combined with the continuity equation (Richards, 1931). Firstly, the Darcy equation will be derived, on whose basis the modified Buckingham-Darcy flux law can be constructed. This is followed by the description of the continuity equation. Finally, these equations will be combined to obtain the Richards equation.

In 1856, the french engineer Henry Darcy developed a physical law describing the water flow in a **saturated** porous sandy soil (Darcy, 1856):

$$Q = \frac{K_s A \Delta P}{L}, \tag{1.1}$$

with Q $[L^3T^{-1}]$, the volume of water flowing per unit time through water-saturated packed sand columns of length L $[L]$ and area A $[L^2]$, when a hydrostatic pressure difference $\Delta P = P_2 - P_1$ $[L]$ is present. The proportionality constant K_s $[LT^{-1}]$, the saturated hydraulic conductivity, represents a uniform constant property for a rigid, saturated soil in a given geometric configuration. In a more general formulation, when gravitational components are considered as well and the flow is expressed as a flux, Eq. (1.1) becomes:

$$J_w = -K_s \frac{h_2 - h_1}{z_2 - z_1}, \tag{1.2}$$

with $J_w = \frac{Q}{A}$ $[LT^{-1}]$ the fluid flux between point 1 and 2. Furthermore, h_i represents the hydraulic head, which is the sum of the hydrostatic head ψ_i $[L]$ and geometric/-gravitational head z_i $[L]$. Using derivative notation, Eq. (1.2) for one dimensional vertical flow can be written as:

$$J_w = -K_s \frac{dh}{dz}. \tag{1.3}$$

Later, in 1907, the american physicist Edgar Buckingham proposed a modification of Darcy's law to describe the flux of water through **unsaturated** soil (Buckingham, 1907). This modification rests primarily on two assumptions:

1. The driving force of water flow in an isothermal, rigid, unsaturated soil containing no solute membranes and zero air pressure potential is the sum of the matric and gravitational potentials;
2. The hydraulic conductivity of an unsaturated soil is a function of the water content or the matric potential.

In head units, the Buckingham-Darcy flux for vertical flow is expressed as:

$$J_w = -K(\psi)\frac{\partial h}{\partial z} = -K(\psi)\frac{\partial(\psi + z)}{\partial z} = -K(\psi)\left(\frac{\partial \psi}{\partial z} + 1\right), \tag{1.4}$$

where $h = \psi + z$ $[L]$ is the hydraulic head and $K(\psi)$ $[LT^{-1}]$ is the unsaturated hydraulic conductivity. J_w $[LT^{-1}]$ is the water flux per unit cross-sectional area per unit of time. Note that Eq. (1.4) is a partial differential equation (PDE), because in unsaturated soil, ψ may be a function of both z and t. If the system is at steady state, the PDE reduces to an ordinary differential equation (ODE), since then ψ depends only on z, i.e.

$$J_w = -K(\psi)\left(\frac{d\psi}{dz} + 1\right). \tag{1.5}$$

In general, wetting or drying of the soil occurs as water flows, and the matric potential and water content will be functions of time as well as of space. Such a transient or time dependent flow, requires a more complete mathematical description than steady-state flow.

The first step to arrive at a complete description of transient water flow is to consider the law of mass conservation at the level of an elementary volume for bare, vegetation-free soil (Figure 1.3):

$$V_{in} = V_{out} + V_{stored}. \tag{1.6}$$

with $V_{entering}$ the volume of water that enters the soil volume ($V = \Delta x \Delta y \Delta z$), $V_{leaving}$ the volume of water that leaves the soil volume and V_{stored} the increase of water volume stored in the soil volume, all during a specific time step Δt.

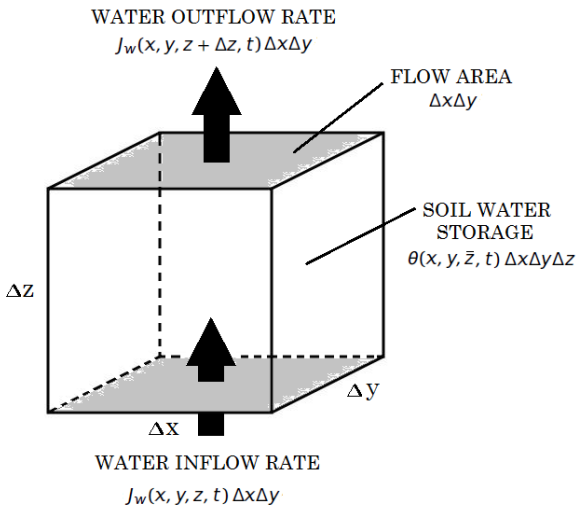

Figure 1.3: Elementary soil volume

For one-dimensional vertical flow process, the volume of water entering the soil volume during Δt is given by:

$$V_{in} = J_w(x, y, z, t + \frac{\Delta t}{2})\Delta x \Delta y \Delta t, \tag{1.7}$$

where J_w $[LT^{-1}]$ is the water flux in the z direction and $\Delta x \Delta y$ is the cross-sectional area of the inflow surface. The flux is taken at $t+\Delta t/2$, this is the average flux between time t and $t + \Delta t$.

Simularly, the volume of water leaving the soil volume during Δt is given by

$$V_{out} = J_w(x, y, z + \Delta z, t + \frac{\Delta t}{2})\Delta x \Delta y \Delta t. \tag{1.8}$$

The increase in water volume (ΔV) stored in the soil volume during Δt can be expressed in terms ov volumetric water content θ $[-]$ as

$$\Delta V = \left[\theta(x, y, z + \frac{\Delta z}{2}, t + \Delta t) - \theta(x, y, z + \frac{\Delta z}{2}, t)\right]\Delta x \Delta y \Delta z, \tag{1.9}$$

where the water content is considered halfway of the volume.

Inserting Eqs. (1.7), (1.8) and (1.9) to Eq. (1.6) gives:

$$\begin{aligned}\Big[J_w(x, y, z, t + \Delta t/2) - J_w(x, y, z + \Delta z, t + \Delta t/2)\Big]\Delta x \Delta y \Delta t = \\ \Big[\theta(x, y, z + \Delta z/2, t + \Delta t) - \theta(x, y, z + \Delta z/2, t)\Big]\Delta x \Delta y \Delta z\end{aligned} \tag{1.10}$$

After dividing this expression by $\Delta x \Delta y \Delta z \Delta t$ and rearranging terms it becomes:

$$\begin{aligned}&\frac{J_w(x, y, z + \Delta z, t + \Delta t/2) - J_w(x, y, z, t + \Delta t/2)}{\Delta z} + \\ &\frac{\theta(x, y, z + \Delta z/2, t + \Delta t) - \theta(x, y, z + \Delta z/2, t)}{\Delta t} = 0.\end{aligned} \tag{1.11}$$

In the limit as $\Delta z \to 0$ and $\Delta t \to 0$ Eq. (1.11) becomes:

$$\frac{\partial J_w}{\partial z} + \frac{\partial \theta}{\partial t} = 0 \tag{1.12}$$

This equation is called the continuity equation for one space and time dimension. If the Buckingham-Darcy flux equation, Eq. (1.4), is now substituted to Eq. (1.12) one obtains the so called Richards equation:

$$\frac{\partial \theta}{\partial t} = \frac{\partial}{\partial z}\left[K(\psi)\left(\frac{\partial \psi}{\partial z} + 1\right)\right]. \tag{1.13}$$

In this form the Richards equation cannot be solved, because it contains two unknowns (θ and ψ) in only one equation. This can be overcome by using the (soil) water retention curve (WRC) $\psi(\theta)$ that eliminates either θ or ψ (Buckingham, 1907). The WRC is a characteristic function which expresses the relationship between the water content, θ, and the soil water potential, ψ. The curve has a unique shape for a given soil type. Since either variable may be eliminated, there are two forms of the equation, the water content form and the matric potential form. From now on, the latter will be used.

The time derivative in Eq. (1.13) can be rewritten using the chain rule:

$$\frac{\partial \theta}{\partial t} = \frac{d\theta}{d\psi}\frac{\partial \psi}{\partial t} \equiv C_w(\psi)\frac{\partial \psi}{\partial t}, \tag{1.14}$$

with

$$C_w(\psi) = \frac{d\theta}{d\psi}, \tag{1.15}$$

the soil water retention capacity $[L^{-1}]$, which equals the inverse slope of the WRC $\psi(\theta)$. It is only defined for uniform wetting or drying processes (van Genuchten, 1980).

Inserting Eq. (1.14) to Eq. (1.13) gives:

$$C_w(\psi)\frac{\partial \psi}{\partial t} = \frac{\partial}{\partial z}\left[K(\psi)\left(\frac{\partial \psi}{\partial z} + 1\right)\right], \tag{1.16}$$

which can be solved if appropriate boundary conditions and an initial condition are specified, given that $C_w(\psi)$ (and thus the WRC $\theta(\psi)$) and $K(\psi)$ are known. These characteristic curves are analytic functions representing global properties of the soil under study. The most widely used functions are those developed by Brooks and Corey (1964):

$$\Theta = \frac{{\psi_a}^{\lambda}}{\psi} \tag{1.17}$$

$$K(\psi) = \frac{{\psi_a}^{\omega}}{\psi} \tag{1.18}$$

from which

$$K(S_e) = \Theta^{\frac{\omega}{\lambda}}, \tag{1.19}$$

$$C_w(\psi) = \frac{\lambda(\theta_s - \theta_r)(-\psi_a)^{\lambda}}{(-\psi)^{\lambda} + 1}, \tag{1.20}$$

Those by van van Genuchten (1980) are also widely adopted and are given by

$$S_e(\psi) = [1 + (-\alpha\psi)^n]^{-m}, \tag{1.21}$$

$$K(\psi) = K_s \frac{1 + (-\alpha\psi)^{n-1}[1 + (-\alpha\psi)^n]^{-m}}{[1 + (-\alpha\psi)^n]^{ml}}, \tag{1.22}$$

from which

$$K(S_e) = K_s S_e^l [1 - (1 - S_e^{\frac{1}{m}})^m]^2, \tag{1.23}$$

$$C_w(\psi) = \frac{\alpha^n(\theta_s - \theta_r)\ m\ n(-\psi)^{n-1}}{[1 + (-\alpha\psi)^n]^{m+1}}, \tag{1.24}$$

with S_e, the effective saturation

$$S_e = \frac{\theta - \theta_r}{\theta_s - \theta_r} \tag{1.25}$$

and

$$\omega = 2 + 3\lambda \tag{1.26}$$

with θ_s $[L^3L^{-3}]$ and θ_r $[L^3L^{-3}]$ the saturated and residual soil-water content, respectively, ω $[-]$, λ $[-]$, α $[L^{-1}]$, n $[-]$, m $[-]$, ψ_a $[L]$ and l $[-]$ are fitting parameters. The parameter n is related to the porosity of the soil and often it is assumed that $m = 1 - 1/n$. l is related to the tortuosity of the soil and is often assumed to be 0.5. Note that ψ_a represents the bubbling pressure (air entry value) and α is the inverse of the air entry value.

Since the expression for $K(\psi)$ or $K(\theta)$ by van Genuchten is derived from a WRC $\theta(\psi)$ using the theoretical pore size distribution model of Mualem (Mualem, 1976), it is generally referred to as the Mualem-van Genuchten (MVG) equation.

Parameters in the soil water retention curves (SWRC) are often determined by curve fitting (Cornelis et al., 2005). Alternatively, inverse methods have been used by fitting numerical solutions of the Richards equation to one-step or multistep outflow data or field data (van Dam et al., 1994). A third method to derive those parameters uses pedotransfer functions, which makes it possible to predict them (indirectly) from readily available soil properties, such as sand, silt, or clay content, organic matter content and bulk density, among others (Vereecken et al., 2010; Botula et al., 2013).

1.2.2 Limitations to the Richards Equation

Note that the Richards equation Eq. (1.16) is coupled and highly nonlinear due to the pressure head dependencies in the specific soil moisture capacity and relative hydraulic conductivity terms ($C_w(\psi)$ and $K(\psi)$). It has no closed-form analytic solution which implies that linearization (such as the Newton-Raphson-, Picard-, modified Picard methods or the L-scheme and combination of them) and iterative methods are needed for obtaining an appropriate numerical solution (Paniconi et al., 1991; Paniconi and Putti, 1994; Knabner and Angermann, 2003; List and Radu, 2016).

Numerically solving the Richards equation has been criticized for being computationally expensive and unpredictable (Short et al., 1995; Tocci et al., 1997), because there is no guarantee that a solver will converge for a particular set of soil constitutive relations (initial and boundary conditions). This hampers its use in applications where the risk of non-convergence is high. It has also been criticized for over-emphasizing the role of capillarity (Germann, 2010) and for being, in some ways, 'overly simplistic' (Gray and Hassanizadeh, 1991). For example, the equation cannot mimic finger-like infiltration in unsaturated homogeneous porous media, a phenomenon that can occur if small amounts of water are added to dry soils (Fürst et al., 2009). However, the dual porosity models by Gerke and van Genuchten (1993) and Jarvis and Larsbo (2012) are capable of simulating complex preferential flow situations using parameters which can be related to physical and chemical properties of the medium. Fürst et al. (2009); Glass and Yarrington (2003) argue that these phenomena could possibly be simulated by other types of models as well such as cellular automata. However, the Richards equation is still relevant and useful to solve specific problems and will probably continue to do so in the near future (Paniconi and Putti, 2015).

1.2.3 Spatio-temporal models (STMs)

Aside from the Richards equation there are other ways to simulate unsaturated flow. Moreover, there exist a bunch of models that have been conceived for simulating all sorts of environmental processes of which most can be classified under spatio-temporal models (STMs). The next section introduces a brief overview of possible modelling approaches. After this orientation, one paradigm will be applied to the a discrete formulation of unsaturated flow to develop a full working model as has been done in Mendicino et al. (2006).

Similar to the classification of spatially explicit models of population dynamics by Berec (2002), STMs can be classified according to whether space, time and state are conceived in a discrete (D) or continuous (C) way. Table 2.1 gives the most common classification of STMs used in literature. It should be mentioned that the nomenclature of STMs is rather ambiguous, as the same mathematical construct is often assigned different labels depending on the scientific discipline and common practice. Furthermore, it should be emphasized that certainly not all models can be named straightforwardly because some of them constitute hybrids between two or more of the listed constructs (Baetens and Nopens, 2016).

Table 1.1: Classification of spatio-temporal models, based on the continuous or discrete nature of the space-time region and state-space (Berec, 2002).

Time	**Space**	**State**	**Name**	**Constructs**
C	C	C	PDE-based model	PDEs
C	D	C	Spatially implicit model	ODEs
D	C	C	Reaction-diffusion model	IdEs
D	D	C	Coupled-map lattice	PdEs
C	C	D	Spatial point model	Set of rules
D	C	D	Agent-based model	Set of rules
C	D	D	Interacting particle system	Set of rules
D	D	D	Cellular automata	Set of rules

One of these approaches are the so-called cellular automata (CA), first proposed in the 50s by John Von Neumann and Stanislaw Ulam (von Neumann, 1966). Since then, new ideas and numerous developments together with the increase of computational power have pushed the original concept to a more mature and robust modeling paradigm as it is known today (Gardner, 1995; Tobler, 1979; Toffoli and Margolus, 1987; Margolus et al., 1986; Wolfram, 1986, 1994). CA use a discrete space-time environment. For each cell in the space-grid a local neighborhood (surrounding cells) is defined to which a transition function is applied to calculate one or more state variables in that cell for the next time step. Transition functions can be based on algebraic (physical) or

empirical equations, expert rules or combinations of the latter, and these can either be deterministic or stochastic (Fonstad, 2006).

The key question: *"Is it really necessary to go from algebraic to differential formulation in order to go back to some other form of finite modelling?"* led to development of the **cell method** or the so called coupled-map lattice (CML) (Tonti, 2001). It is another numerical procedure for the solution of field equations that relies on partial **difference** equations (PdEs). The essence of the method is to directly provide a discrete formulation of field laws, without requiring a differential formulation. It sufficies to apply the elementary physical laws to small regions, where the uniformity of the field is attained to a sufficient degree, this being linked to the degree of accuracy of input data and to the observation scale of the physical phenomenon (Tonti, 2001). This method has been applied in several scientific branches, including: finite formulation of electromagnetic fields (Tonti, 2002), crack propagation modeling (Ferretti, 2003), two-dimensional estimate of effective properties of solid random voids (Cosmi, 2004), electrodynamics (Cosmi, 2005; Tonti and Zarantonello, 2010), shear test modeling (Ferretti et al., 2003), soft core plane state structures under static loads (Viola et al., 2013) and the simulation of cohesive fractures and fragmentation of continious media (Cusatis et al., 2017).

1.3 An unsaturated flow model based on the Cell Method

1.3.1 Description

In Mendicino et al. (2006) and Folino et al. (2006) a three-dimensional unsaturated flow model based on the cell method concept is proposed. The model consitutes an extension to the original CA paradigm, because it uses a local transition function with a clear physical meaning to govern the interactions among the cells. The aim of this model is to simulate large-scale systems. It includes functionalities capable of increasing its computational capacity, both in terms of working environment and in terms of the optimal number of processors available for parallel computing. The researchers also carried out a validation by comparing the simulation results with reference multidimensional numerical solutions taken from benchmarks in literature (Paniconi et al., 1991; Paniconi and Putti, 1994; Huyakorn et al., 1984). These showed a good agreement, even when non linearity was very marked. Furthermore, the model was updated with a quantization technique that transforms the model into an asynchronous structure (Zeigler, 1998). This means when the driving force of wa-

ter transport between two adjacent cells is negligible, there will be no exchange. The use of this technique in a (quasi) three-dimensional benchmark allowed a considerable reduction in the number of local interactions among adjacent cells characterized by scarce mass exchanges. Furthermore, the model has been coupled to a vegetation dynamic model simulating soil vegetation interactions (Cervarolo et al., 2011).

1.3.2 Model development

This formulation is constructed from the mass balance equation and the constitutive equation (Darcy's law), which leads to the Richards equation (Mendicino et al., 2006). The discrete mass balance equation is given by

$$\sum_{N_i} \Phi^i_{N_i} + \frac{1}{\rho_i} \frac{\Delta m_i}{\Delta t} = S_i, \tag{1.27}$$

with i the cell where the water mass balance is computed, N_i the neighborhood of the center cell i, consisting of the adjacent cells: $N_i = \{j | d_{ij} \leq 1\}$, with d_{ij} the graph distance from i to a neighboring cell j. In this particular case, one uses a three-dimensional von Neumann neighborhood (Figure 1.4).

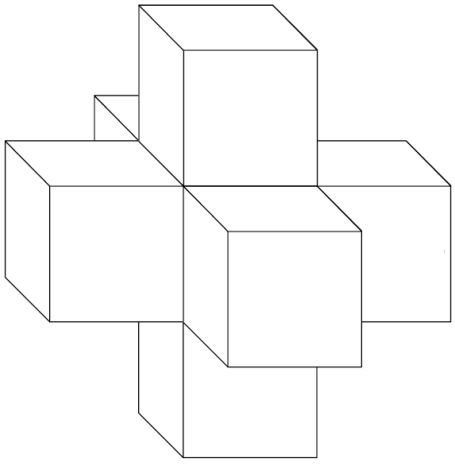

Figure 1.4: The center cell i and its environment N_i after Mendicino et al. (2006)

$\Phi^i_{N_i}$ in Eq. (1.27) is the mass flux $[L^3T^{-1}]$, ρ_i is the fluid density $[ML^{-3}]$, m_i is the mass inside the single cell i $[M]$, Δt is the time step $[T]$, $\frac{\Delta m_i}{\Delta t}$ is the mass-time variation in the cell, and S_i is the mass source term $[L^3T^{-1}]$. Equation (1.27) is valid for both internal nodes of the discrete domain and boundary nodes, avoiding the typical differential approach where differential equations and boundary conditions are separeted. The mass flux is given by Darcy's law, which in discrete terms for a cubic regular mesh becomes:

$$\Phi^{i}_{N_i} = -\overline{K_{N_i}}\left(\frac{h_{N_i} - h_i}{l_{N_i}}\right)A_{N_i}, \tag{1.28}$$

where $\overline{K_N}$ $[LT^{-1}]$ is the hydraulic conductivity averaged between cell i and an adjacent cell j in N_i, obtained by hypothesizing that the energy dissipated between two adjacent cells is equivalent to the energy in a fictious cell containing them (Indelman and Dagan, 1993). If we consider the hydraulic conductivity averaged between cell i and j, we assume

$$\overline{K_{ij}} = \frac{V_i + V_j}{\frac{V_i}{K_i} + \frac{V_j}{K_j}}, \tag{1.29}$$

with V_i and V_j $[L^3]$ the volumes of cell i and j respectively, while K_i and K_j are the elements on the diagonal of the hydraulic conductivity tensor corresponding to the direction ij, assuming that the xyz Cartesian coordinate system is colinear with the principal anisotropy directions. When V_i and V_j are equal Eq. (1.29) reduces to the normal average of K_i and K_j.

The remaining terms in Eq. (1.28) are the total head h_i and the heads of the neighboring cells h_{N_i} $[L]$, the distance between cell i and j l_{N_i} $[L]$ and the surface area A_{N_i} $[L^2]$ where the flux $\Phi^{i}_{N_i}$ passes through. Equation (1.29) is a particular form of a more general direct discrete formulation of the unsaturated flow equation (Mendicino et al., 2006).

For unsaturated flow, assuming the fluid is incompressible and density-independent, the mass time-variation becomes

$$\frac{\Delta m_i}{\Delta t} = V_i \rho_i \frac{\Delta \theta_i}{\Delta t}. \tag{1.30}$$

If the ratio between capillary pressure p_i $[ML^{-1}T^{-2}]$ and the specific weight of the liquid γ_w $[ML^{-2}T^{-2}]$ represents the pressure head ψ_i $[L]$, and the specific retention capacity $C_i(\psi)$ $[L^{-1}]$ is considered (Bear, 1972), then applying the chain rule to $\frac{\Delta\theta}{\Delta t}$ in Eq. (1.30) one obtains:

$$\frac{\Delta \theta_i}{\Delta t} = \frac{\Delta \theta}{\Delta h_i}\frac{\Delta h_i}{\Delta t} = C_i \frac{\Delta h_i}{\Delta t}. \tag{1.31}$$

By inserting Eq. (1.31) in to Eq. (1.30), and substituting the resulting equation together with Eq. (1.28) in Eq. (1.27), one obtains the complete form of the unsaturated soil flux equation:

$$\sum_{N_i} -\overline{K_{N_i}} \left(\frac{h_{N_i} - h_i}{l_{N_i}} \right) A_{N_i} + V_i C_i \frac{\Delta h_i}{\Delta t} = S_i. \tag{1.32}$$

The gravitional potential is embedded in the total head component: $h_i = \psi_i + z_i$, and thus $h_j - h_i = (\psi_j - \psi_i) + (z_j - z_i)$. This discrete unsaturated flow equation can be applied to each cell of the domain with Δh_i the only unknown to be determined. This quantity indicates the total head variation in cell i between instants t and $t + \Delta t$, and can be obtained by expanding Eq. (1.32), which leads to the following expression:

$$\Delta h_i = \frac{\Delta t}{V_i C_i} \left[S_i + \sum_{N_i} -\overline{K_{N_i}} \left(\frac{h_{N_i} - h_i}{l_{N_i}} \right) A_{N_i} \right]. \tag{1.33}$$

To obtain Δh_i it is necessary to specify the nonlinear dependencies among the assumed independent variable, the total head h_i, and terms characterizing the hydraulic properties of soil represented by water content θ_i, specific retention capacity $C_i(\psi_i)$ and hydraulic conductivity $K_i(\psi_i)$. Such relationships are usually expressed through emperical equations fitting experimental data using theoretical models, such as the Brooks and Corey or the MVG model: Eq. (1.17) - (1.26).

$$\Delta h_i = \frac{\Delta t}{V_i C_i(\psi_i)} \left[S_i + \sum_{N} -\overline{K_N}(\psi_i) \left(\frac{h_N - h_i}{l_N} \right) A_N \right]. \tag{1.34}$$

All together, the new value of the total head in cell i at time $t + \Delta t$ becomes:

$$h_i(t + \Delta t) = h_i(t) + \Delta h_i. \tag{1.35}$$

This equation applies to each cell of the grid. An example of the fluxes affecting the amount of water in the center cell is given in Figure 1.5.

1.3.3 General workflow

The complete algoritm of the model is illustrated in Figure 1.6 and is similar to solving the Richards equation numerically. One starts with defining initial conditions (total head h, pressure head ψ, hydraulic conductivity $K(\psi)$ and water content values θ) and the boundary conditions. Then, two elemtary steps follow. Firstly, the updating of the characteristic equations or SWRC. The θ and K values are calculated with the van Genuchten WRC equations (Eq. (1.21) - (1.26)). Here, they are expressed in the form as suggested in van Genuchten and Nielsen (1985):

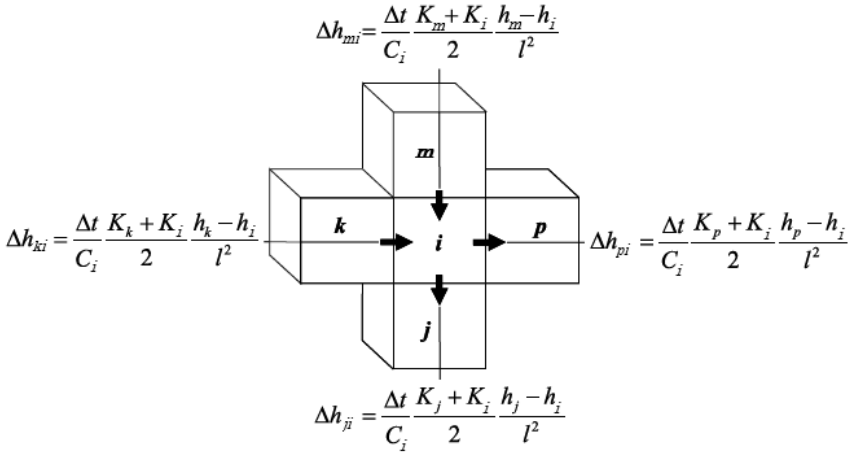

Figure 1.5: Example of interactions of cell i with its neigborhood cells N_i in a bi-dimensional infiltration case after Folino et al. (2006)

$$\theta(\psi) = \begin{cases} \theta_r + (\theta_s - \theta_r)[1+\beta]^{-m}, & \psi < 0, \\ \theta_s, & \psi \geq 0 \end{cases} \tag{1.36}$$

and

$$K_r(\psi) = \begin{cases} (1+\beta)^{-5m/2}[(1+\beta)^m - \beta^m]^2, & \psi < 0, \\ 1, & \psi \geq 0. \end{cases} \tag{1.37}$$

with $\beta = (\psi/\psi_\alpha)^n$ and $K_r(\psi)$ $[-]$ the relative hydraulic conductivity so that $K(\psi)$=$K_s K_r(\psi)$, with K_s $[LT^{-1}]$ the saturated conductivity. Secondly, the unsaturated soil flux equation is applied to all cells (Eq. (1.34) and (1.35)) to update the values of h_i and Ψ_i. Starting the simulation, the other substates conditions ($\theta(\psi)$, K_r and C) depend on the initial values assigned to the total head, while the boundary conditions can be assigned either in terms of mass flow coming in (infiltration) or out (exfiltration) from the system (Neumann conditions), or fixing the total or pressure head values on some cells of the system (Dirichlet conditions). A simulation can be ran for a specific time interval or for a given treshold (for example, if between each cell in the grid the water exchange becomes lower than a certain value i.e. steady state, than the simulation terminates).

1.4 Other CA based flow models

Ravazzani et al. (2011) proposed another CA based model for simulating groundwater flow. This CA is based on a regular grid that represents 2D groundwater flow in

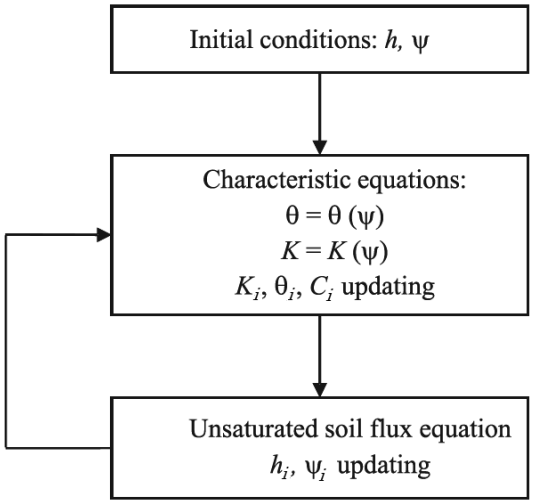

Figure 1.6: Algorithm of the transition functions permitting the evolution of the cells after (Mendicino et al., 2006).

a unconfined aquifer. Physically based equations are implemented to simulate the flow of water between adjacent cells. This model can account for sources or sinks and boundary conditions of Dirichlet or Neumann type. River-aquifer interaction can be simulated: the stream stage is used to calculate the flux between the stream and aquifer system, proportional to the head gradient between the river aquifer and a streambed conductance parameter. Tests of the model under hypothetical conditions showed that the model is stable and convergent when the time step satifies a convergence criterion. The accuracy of the model was evaluated considering three tests, both in transient and steady state: the steady flow between two streams in response to uniform recharge, the drawdown due to a constant pumping rate from a well (Theis, 1935), and the aquifer response to stream-stage variation. Comparison with the analytical solutions and MODFLOW-2000 (Waterloo hydrologic, MODFLOW 4.2) (McDonald and Harbaugh, 1988) numerical results showed a good agreement. The code of this model is simple enough to facilitate its integration into other models, such as distributed models that simulate water and energy fluxed at the interface between soil and atmosphere. The good performance in terms of computation time without detriment to model's accuracy makes this model adequate to perform long simulation periods. However, the motivation for its development was the simulation of unconfined aquifers and their interactions with surface water; it is not intended for the simulation of 3D fluxed in complex and heterogenous stratified confined aquifers.

A synchronous CA model of mass transport in porous media is presented by Gurikov et al. (2016). This paper is less related to the topic of groundwater flow, but nevertheless interesting because of the concepts that are dealt with. The model is a fully synchronous coarse grained CA model for large-scale simulations at molecular level.

It is based on the Margolus partitioning scheme (Toffoli and Margolus, 1987), which was generalized as to quantitatively describe diffusion, adsorption and directed flow in porous media. The original version of the Margolus scheme described molecular diffusion of an ideal gas. This work extended the scheme by introducing thermodynamic considerations in terms of free energy and local equilibrium. Phenomena like diffusion, adsorption, directed flow and chemical reactions are all described in a unified way considering independent rotations of 2 x 2 blocks of the lattice so that synchronicity of the original model is remained. Quantitative agreement between simulation and theoretical solutions are obtained for several diffusion problems, monolayer adorption and retention in chromatography.

In Anagnostopoulos and Burlando (2012) the concepts of the aforementioned model (subsections 1.3.1 - 1.3.3) are extended. The main drawback of the CA model presented in Mendicino et al. (2006) is the fact that the time step depends on the spatial grid and the hydraulic properties of the cells, obeying a specific condition for the algorithm to be convergent. This restriction can increase the computational burden dramatically when large scale problems are examined with unfavourable soil hydraulic properties and boundary conditions, which is often the case in catchment hydrology. Their new computational procedure of the modelling is unconditonally stable, which makes the selection of the time step independent of the grid size and the hydraulic properties. However, the convergence of the algorithm alone does not guarantee that the mass balance errors and the accuracy are kept at acceptable levels, especially in cases where strong non linearities exist (very dry and near saturation conditions). An iteration procedure combined with an efficient (in terms of accuracy and computational burden) convergence criterion (Huang et al., 1996) is used to handle efficiently these cases. The SWRC used are those by van Genuchten and modified van Genuchten that improve accuracy and convergence at the cells near saturation (Vogel et al., 2001; Ippisch et al., 2006; Schaap and van Genuchten, 2005) and the Brooks and Corey model. Furthermore, the performance of various approximations for the internodal conductivities is investigated. The best results were achieved by a model that is based on the steady state distribution of the potential head and distinguishes between thre major cases of the shape of the head profile (Szymkiewicz, 2009). Finally, the model was succesfully tested against 2D infiltration and drainage experimental data in homogeneous and heterogeneous soils and against a 3D analytical solution for simple boundary and initial conditions.

CHAPTER 2

MODEL IMPLEMENTATION AND BENCHMARKING

2.1 Introduction

In Mendicino et al. (2006) no validation with a real field experiment data set is carried out. This is the main objective of this dissertation. However, first the model has to be implemented on a computer for which we chose Wolfram language, available in *Wolfram Mathematica 11* (Wolfram Mathematica, 2018). This environment is a more universal and well-known program than the original model environment i.e. 'CAMELot' (Dattilo and Spezzano, 2003; Mendicino et al., 2006; Folino et al., 2006). Once implemented, one needs to validate numerical results against solutions of the original model to check whether the model works appropriately.

2.2 Benchmarking

2.2.1 One-Dimensional Benchmarks

Two one-dimensional benchmarks were considered along two different soil colums (Paniconi et al., 1991). These benchmarks were used in Mendicino et al. (2006) to validate the model against numerical results of Paniconi et al. (1991), here they were implemented again in Mathematica. The first one is an infiltration problem, the second one an evaporation problem. Both cases are based on the unmodified Richards' equation. The results of the CML model are compared to those produced by the model of Mendicino et al. (2006).

The characteristic equations taken into account for these simulations are Eq. (1.37) and a modified version of Eq. (1.36), i.e.

$$\theta(\psi) = \begin{cases} \theta_r + (\theta_s - \theta_r)[1+\beta]^{-m}, & \psi < \psi_0, \\ \theta_r + (\theta_s - \theta_r)[1+\beta_0]^{-m} + S_s(\psi - \psi_0), & \psi \geq \psi_0, \end{cases} \tag{2.1}$$

with $\beta_0 = \beta(\Psi_0) = (\Psi/\Psi_a)^n$ $[-]$, Ψ_0 $[L]$ and S_s $[L^{-1}]$ continuity parameters and S_s the specific storage. The general storage term of the Richards' equation is given by Eq. (1.15) and thus gives:

$$C_w(\psi) = \begin{cases} (-m)(\theta_s - \theta_r)\left[1 + \left(\frac{\psi}{\psi_a}\right)^n\right]^{-m-1} n\left(\frac{\psi}{\psi_a}\right)^{n-1}\left(\frac{1}{\psi_a}\right), & \psi < \psi_0, \\ S_s, & \psi \geq \psi_0. \end{cases} \tag{2.2}$$

The modified water content equation, Eq. (2.1), is to avoid numerical problems, such as those indicated by Paniconi et al. (1991). However, as will be shown later, this is one of the main drawbacks of the model.

Benchmark 1D1

Benchmark 1D1 simulates the infiltration and redistribution of water into a soil column initially at hydrostatic equilibrium. The boundary condition at the surface is a time-varying Darcy flux q $[LT^{-1}]$ which increases lineary with time, while the boundary at the base is maintained at a fixed pressure head of $\Psi = 0$, allowing drainage of moisture through the water table. The spatial discretization and time step were chosen to guarantee convergence, following the guidelines given in Mendicino et al. (2006). It should hold that:

$$\Delta t \leq \frac{l^2 C^t_{i,j,k}}{\overline{K^t}_{i\pm1,j\pm1,k\pm1}}, \tag{2.3}$$

with l the cell dimension , $C_{i,j,k}$ the retention capacity of an individual cell i,j,k at time t and $\overline{K^t}_{i\pm1,j\pm1,k\pm1}$ the sum of the hydraulic conductivities averaged between the cell i,j,k and the adjacent points $i \pm 1, j \pm 1, k \pm 1$ at time t. Note that if the retention capacity approaches zero, convergence cannot be guaranteed because Δt declines as well. This criterion holds for each of the simulations presented in the remainder.

The parameters used in Mendicino et al. (2006) for the 1D1 benchmark are shown in Table 2.1. Only their values of S_s and Ψ_0 (the continuity parameters) were changed from those proposed by Paniconi et al. (1991), because of the convergence condi-

tions for a time step equal to 0.1 s. During their simulations they observed that small changes of Ψ_0 did not affect the final result. However, in the CML model presented here, again a change of those continuity parameters was necessary in order to guarantee convergence. This matter is discussed below. The pseudocode of the model is given in Algorithm 1.

Table 2.1: Parameters for Benchmark 1D1 used by Mendicino et al. (2006) and the CML model used here

Parameter	**Mendicino 2006**	**CML Model**	**Units**
θ_r	0.08	0.08	-
θ_s	0.45	0.45	-
ψ_a	-3.0	-3.0	m
n	3.0	3.0	-
S_s	0.02347	**0.026**	m^{-1}
ψ_0	-0.95	**-0.9999**	m
K_s	1.389 x 10^{-3}	1.389 x 10^{-3}	ms^{-1}
Surface boundary condition	q = t/64	**q = t x 0.00434**	ms^{-1}
Height of the soil column	10.0	10.0	m
Δz	0.1	0.1	m
Δt	0.1	0.1	s

Algorithm 1: Algorithm of the CML model for simulating benchmark 1D1

Data: θ_r, θ_s, ψ_a, n, K_s, q, S_s, ψ_0 and z

Result: h, ψ-, K-, θ- and C_w profiles

Initial conditions: $h_{initial}$ and $\psi_{initial}$;

t $\leftarrow$ 0;

t_{end} = simulation time;

$K(t = 0)$ (Eq. 1.37);

$C_w(t = 0)$ (Eq. 2.2);

$\theta(t = 0)$ (Eq. 2.1);

while $t \leq t_{end}$ **do**

  for $x = 2 : z - 1$ **do**

    $h(x, t) = h(x, t-1) + \Delta h(x)$;

  end

  $h(z, t) = h(z, t-1) + q(t)$;

  $h(1, t) = 0$;

  $\psi = h\text{-}z$;

  $K(t)$;

  $C_w(t)$;

  $\theta(t)$;

end

Figure 2.1 gives the pressure head profiles obtained after 0, 1, 2, 4, 10 and 32 hours using the parameter values in Table 2.1 and compares them with the results of Mendicino et al. (2006).

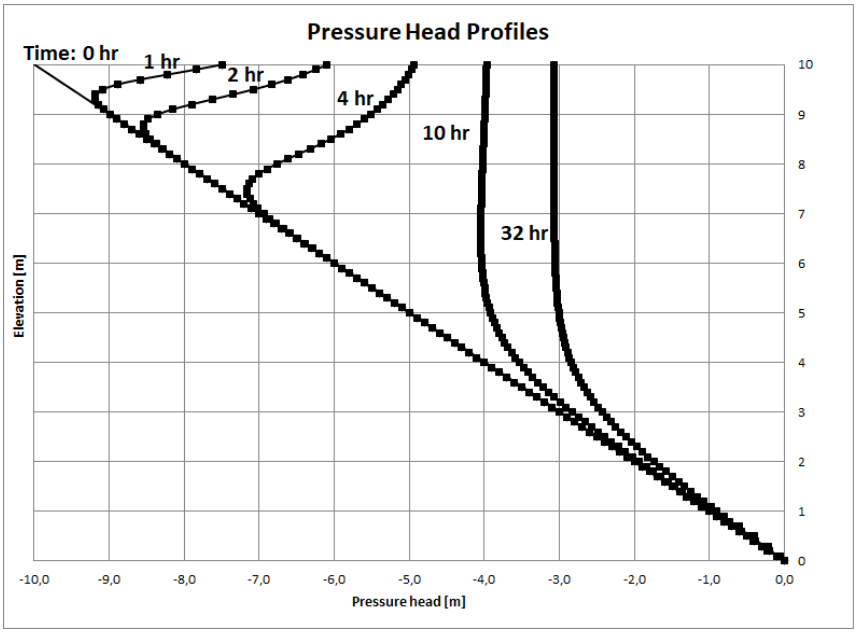

Figure 2.1: Pressure head profiles obtained with our model implementation (squares) of the CML model proposed by Mendicino et al. (2006) and theirs (full lines) for the 1D1 benchmark at 1, 2, 4, 10 and 32 hours.

It is a bit hard to see, but in Figure 2.1 a convergence problem occurs near the GWT at a simulated period of 32 hours. This problem first occured at lower simulation times as well; but the continuity parameters (S_s and Ψ_0) were adjusted manually to solve this issue for shorter simulated periods. However, it popped up again at a simulation time of 32 hours. The cause for this issue could be traced back to the convergence criterion Eq. (2.3), which might not be fulfilled at local cells near the GWT.

The hydraulic conductivity, water retention, water content and WRC profiles for a simulated period of 32 hours are given in Figure 2.2. On the water retention capacity profile (C_w) the influence of the continuity parameters can be seen. Indeed C_w becomes 0.026 m^{-1} if $\psi \geq \psi_0$ as described in Eq.(2.2).

In Table 2.2 the corresponding computing times (CPU timing) are given. The simulations were executed on an HP Pavilion Entertainment Laptop type dv6-1300sb with a Pentium Dual-Core CPU T4300 at 2.10 Ghz (2CPUs).

Table 2.2: Computing time (in seconds) for the simulations for the 1D1 benchmark

1 hour	**2 hours**	**4 hours**	**10 hours**	**32 hours**
274,8	538,6	1102,4	2799,1	8907,1

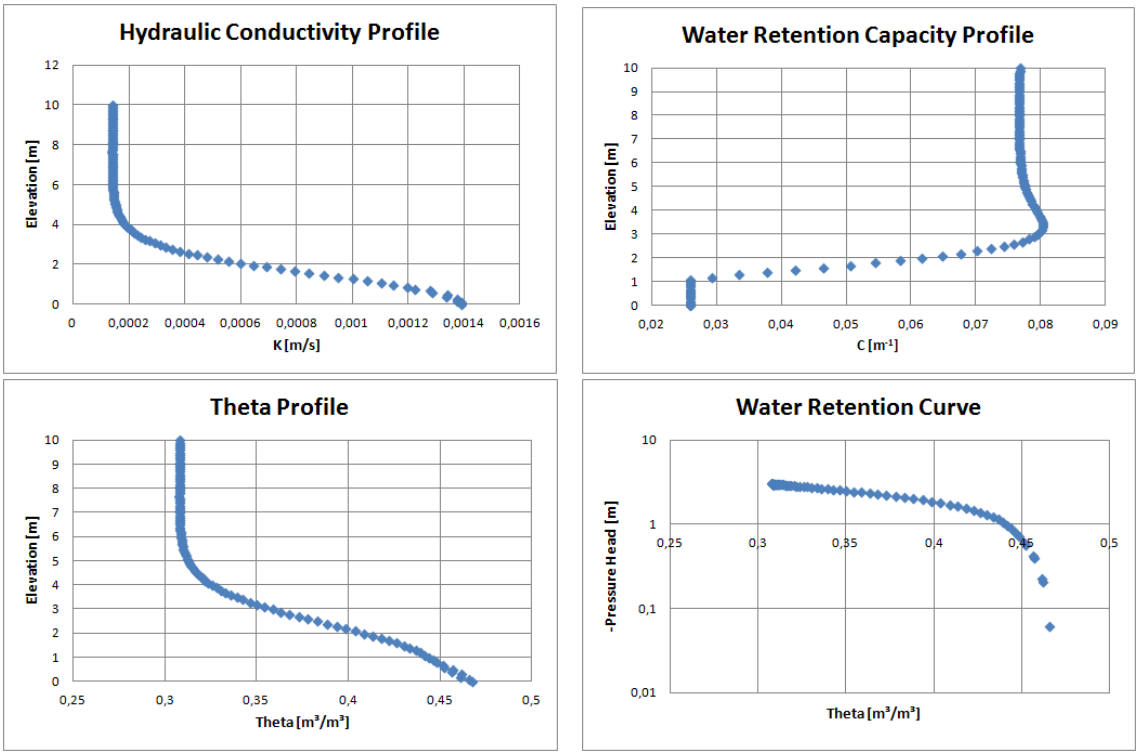

Figure 2.2: Hydraulic conductivity, water retention, water content and WRC profiles Benchmark 1D1 for a simulated period of 32 hours

Benchmark 1D2

Benchmark 1D2 concerns the evaporation from an initially wet soil with a fixed water table at the base of the column. The boundary condition at the surface is a constant Darcy flux, until the pressure head at the surface reaches its air dry value ψ_{min}, after which the surface becomes a fixed head boundary. The parameters used in Mendicino et al. (2006) for this benchmark are shown in Table 2.3. The continuity parameters had to be changed in order to avoid convergence problems.

Table 2.3: Parameters for Benchmark 1D2 used by Mendicino et al. (2006) and the CML model

Parameter	**Mendicino 2006**	**CML model**	**Units**
θ_r	0.15	0.15	-
θ_s	0.38	0.38	-
ψ_a	-1.2	-1.2	m
n	4	4	-
S_s	0.0001	**0.0010**	m^{-1}
ψ_0	-0.06698246	**-0.1**	m
ψ_{min}	-1.75	-1.75	m
K_s	2.778 x 10^{-6}	2.778 x 10^{-6}	ms^{-1}
Surface boundary condition	q = -0.0006, then $\psi = \psi_{min}$	adjusted (see text)	?
Height of the soil column	5.0	5.0	m
Δz	0.05	0.05	m
Δt	0.1	0.1	s

Figure 2.3 gives the pressure head profiles obtained after 0, 1, 3, 12, 24 and 45 hours using the parameter values in Table 2.3 and compares them with those obtained by Mendicino et al. (2006). In Table 2.4 the corresponding computing times are given.

As can be seen on Figure 2.3 , the simulated pressure head profiles do not always match. The pressure heads in the CML model differ at a simulated periods of 24 and 45 hours. The reason for this resides in a deviation from the original boundary flux (see Table 2.3). The units for the Darcy boundary flux were not given in Mendicino et al. (2006), so these were adjusted manually until there was a match.

Table 2.4: Computing time (in seconds) for each of the simulations of the 1D2 benchmark

1 hour	**3 hours**	**12 hours**	**24 hours**	**48 hours**
308,8	871,1	3255,5	6554,6	12404,3

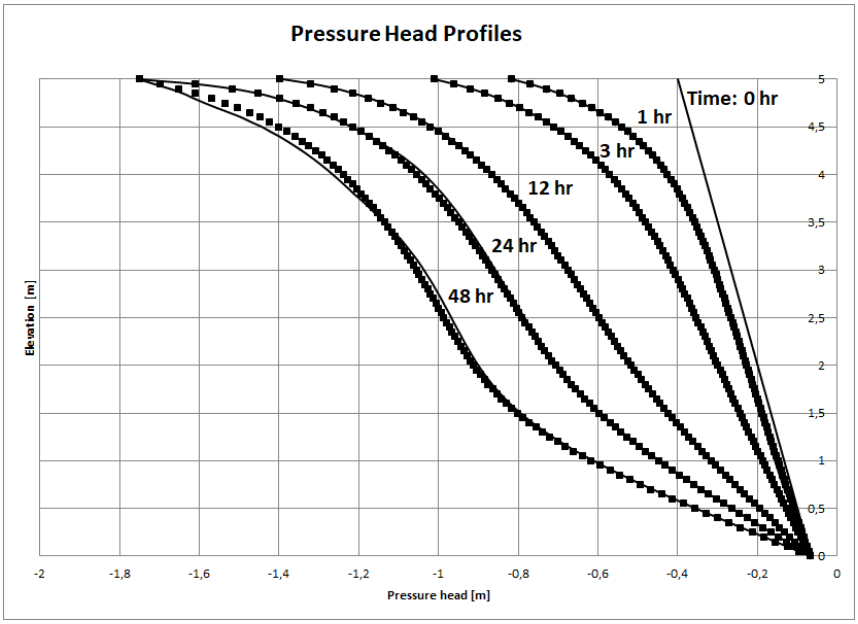

Figure 2.3: Pressure head profiles obtained with our model implementation (squares) of the model proposed by Mendicino et al. (2006) and theirs (full lines) for the 1D2 benchmark at 1, 3, 12, 24 and 48 hours.

2.2.2 Two-Dimensional Benchmark

The two-dimensional benchmark was taken from Paniconi and Putti (1994). It concerns infiltration in transient conditions. The characteristic equations are those of Huyakorn et al. (1984), in which water saturation S_w [−] is expressed in terms of effective saturation S_e [−]:

$$S_w = (1 - S_{wr})S_e + S_{wr}, \tag{2.4}$$

with S_{wr} (θ_r/ϕ) [−] the residual water saturation. The characteristic equations then become

$$S_e(\psi) = \begin{cases} [1 + \alpha^\beta(\psi_a - \psi)^\beta]^{-\gamma}, & \psi < \psi_a, \\ 1, & \psi \geq \psi_a, \end{cases} \tag{2.5}$$

and

$$K_r = K_r(S_e(\psi)) = S_e^n, \tag{2.6}$$

with ϕ the porosity [−], ψ_a [L] the air entry pressure, and α [−], β [−], γ [−], and n [−] are constants. The general storage term in this case is given by

$$C_w = S_w S_s + \phi \frac{dS_w}{d\phi}. \tag{2.7}$$

This benchmark simulates transient flow in an unsaturated soil slab with very low initial pressure head values. The combination of soil parameters (Table 2.5) with the initial condition produces a moving front, where highly variable values of relative hydraulic conductivity and saturation require a little care to obtain convergence and stability. Again, a treshold value of ψ_0 has been fixed. If it is exceeded, the term relative to the specific retention capacity is constant. Consequently, Eq. (2.5) becomes:

$$S_e(\psi) = \begin{cases} \left[1 + \alpha^\beta(\psi_a - \psi)^\beta\right]^{-\gamma}, & \psi < \psi_0, \\ \left[1 + \alpha^\beta(\psi_a - \psi)^\beta\right]^{-\gamma} + S_e(\psi - \psi_0), & \psi_0 \leq \psi < \psi_a, \\ 1, & \psi \geq \psi_a, \end{cases} \tag{2.8}$$

The derivative of Eq. (2.7) with respect to ψ is expressed as:

$$\frac{dS_w}{d\psi} = \begin{cases} (1-S_{wr})(-\gamma)\left[1+\alpha^{\beta}(\psi_a-\psi)\right]^{-\gamma-1}\left[\alpha^{\beta}\beta(\psi_a-\psi)^{\beta-1}\right], & \psi < \psi_0, \\ S_{se}, & \psi_0 \leq \psi < \psi_a, \\ 0, & \psi \geq \psi_a. \end{cases} \quad (2.9)$$

Table 2.5: Parameters for Benchmark 2D used by Mendicino et al. (2006) and the CML model

Parameter	**Mendicino 2006**	**CML Model**	**Units**
ψ_a	0	0	m
α	-0.01	-0.01	-
β	3	3	-
γ	-3	-3	-
n	4	4	-
S_{wr}	1/3	1/3	-
ϕ	0.45	0.45	-
S_s	0	**0.6**	-
ψ_0	-0.14	-0.14	m
S_{se}	0.00001754	0.00001754	m
K_s	1.157 x 10^{-5}	1.157 x 10^{-5}	ms^{-1}
L_x	0.15	0.15	m
L_z	0.10	0.10	m
$\Delta z = \Delta x$	0.01	0.01	m
Δt	0.1	0.01	s
Initial conditions	$\psi(x, z, 0)$ = -0.90	$\psi(x, z, 0)$ = -0.90	m
Boundary conditions	$\psi(0, 6-10, t)$ = 0.60 - z; $\psi(0, 15, 0-10, t)$ = -0.90	$\psi(0, 6-10, t)$ = 0.60 - z; $\psi(0, 15, 0-10, t)$ = -0.90	m

In Figure 2.4 the results reported by Mendicino et al. (2006) are compared to the benchmark in Paniconi et al. (1991). The lines and dashed lines represent the value of the pressure head (ψ in cm). However, as one can see in Table 2.5 the spatial discretisation is 1 cm and the pressure head values are far more accurately, so it seems that the numerically obtained pressure head values were interpolated lineary.

For simulating this benchmark with the CML model, the continuity parameter S_s had to be changed. Overflow in computation immediately occured when S_s was kept at the original value of 0. The reason for this can be traced back to general storage term Eq. (2.7). When this value becomes zero, the unsatured soil flux equation blows up to infinity, because there is a zero term in the denominator. It is unclear how Mendicino et al. (2006) got to a meaningful result if S_s was zero, anyway it was changed to 0.6 in the CML model. The results are given in Figure 2.5 for a simulated period of 32 hours. A simulated period of 5 days gave the same result, indicating that at 32 hours the steady-state had already been reached. The pressure head values do not match those in Figure 2.4, which is due to the higher S_s value that tends to slow down the moving front considerably.

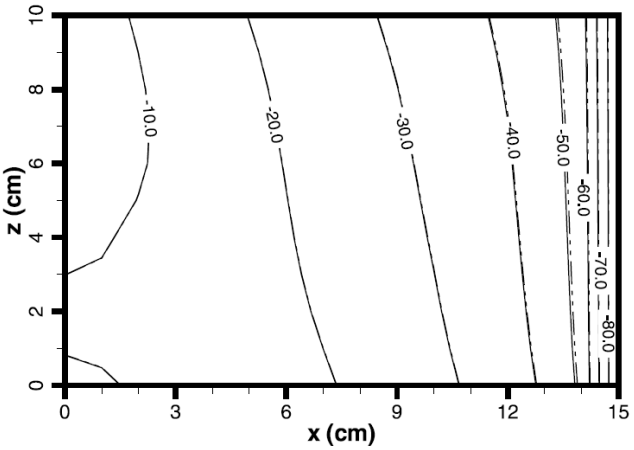

Figure 2.4: Pressure head contour plots obtained with the model implementation of Mendicino et al. (2006) (solid lines) and the reference numerical solutions of Paniconi et al. (1991) (dashed lines) at a simulated period of 5 days.

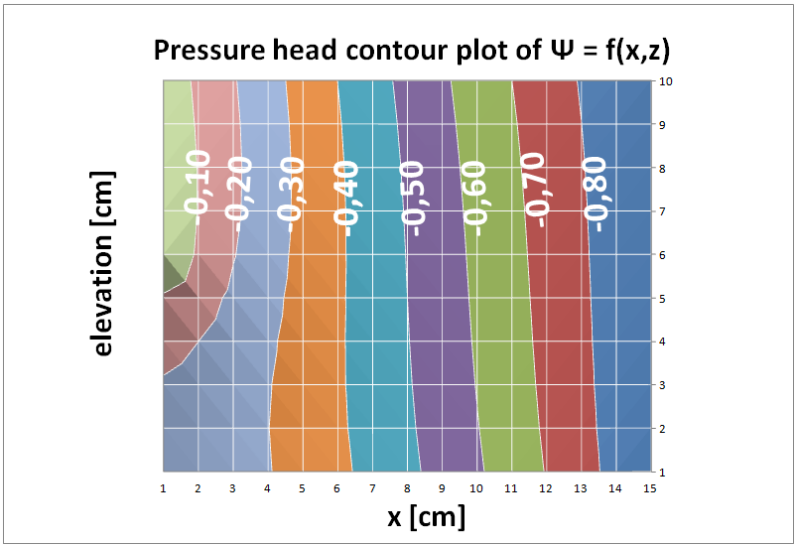

Figure 2.5: Interpolated pressure head contour plot for a simulated period of 32 hours with the 2D CML model, the pressure head is expressed in m.

In Table 2.6 the corresponding computing times (CPU timing) are given.

Table 2.6: Computing time (in seconds) for the 2D benchmark

1 hour	2 hours	4 hours	10 hours	32 hours
435,8	899,6	1729,0	4501,0	14040,0

CHAPTER 3

GLOBAL SENSITIVITY ANALYSIS AND VALIDATION

This chapter aims at assessing the performance of the model. The assessment is twofold, as it involves a global sensitivity analysis (GSA) and a validation.

3.1 Global Sensitivity Analysis (GSA)

3.1.1 Introduction

A sensitivity analysis (SA) is the study of how uncertainty in model outputs is determined by uncertainty in model inputs. A GSA considers the potential effects from the simultaneous variation of model inputs over their finite range of uncertainty. The use of models, in particular in the environmental domain, inevitably involves the presence and treatment of uncertainties. The input of a model is subject to many sources of uncertainty including errors of measurement, the absence of information, sampling design, out-of-date information, scaling errors, and poor or partial understanding of the driving forces and mechanisms (model conceptual uncertainty) (Burrough and McDonnel, 1998). This imposes a limit on our confidence in the response of the model. Uncertainty and SA are potentially able to increase confidence in the model and its predicitions, by providing an understanding of how the model respons varies to changes in the input (Lilburne and Tarantola, 2009; Saltelli et al., 2008).

While uncertainty analysis quantifies the magnitude of the resulting uncertainty in the model outputs due to uncertainties in model inputs, SA is the study of how the uncertainty in the output of the model can be apportioned to different sources of uncertainty in the model inputs (Saltelli et al., 2008). The aim of a local SA is to quantify the rate of change of the model output due to small variations in the uncertain model inputs. GSA methods consider the full ranges of uncertainty of the inputs, which are characterised via their joint probability density functions (pdf) (Lilburne and Tarantola, 2009).

A number of techniques are available to carry out GSAs from a set of Monte Carlo simulations; some techniques are more efficient than others, depending on the strategy used to sample the uncertainty of model inputs and on the formulae employed for estimating sensitivity measures (Lilburne and Tarantola, 2009).

3.1.2 Method

A general GSA consists of six steps (Lilburne and Tarantola, 2009):

1. Specify the target function(s) of the study.
2. Select the inputs of interest.
3. Assign a range and a statistical distribution to the selected inputs.
4. Apply a sampling design to generate a sample size N from the distributions of the inputs.
5. Evaluate the model for each sample set of input values obtaining N values for the target function(s).
6. Use the results of step 5 for uncertainty analysis and apply an estimator of sensitivity to obtain the relative importance of the inputs.

Method applied

Here, the target functions are the output of the model namely the pressure head profile, $\Psi(z)$ for an infiltration experiment similar to benchmark 1D1. However, the whole profile cannot be taken as a single estimator so one must find one or more parameters who contain information on the shape of the profiles. These parameters are called fitting parameters, because one can fit a curve that approximates the original pressure head profile using these parameters. The first fitting parameter was chosen to be the minimal pressure head value of the profile, ψ_{MIN}. This is, most of the time, the point where the pressure head profile makes a bend (see Figure 2.1). The second, the pressure head at the soil atmosphere interface, ψ_b. Notice that in some cases ψ_{MIN} and ψ_b are the same, for example at a simulated period of 32 hours. The pressure head at the GWT would not be a good fitting parameter, because this value is fixed at $\psi = 0$ m. The last parameter is not a fitting parameter, it is the sum of the water contents, θ_{TOT}, over the whole column. This value indicates how much moisture is present in the column and thus contains information on how much the curve is shifted to the right or left. For example, when the curve is shifted to the right, and thus approaches

$\psi = 0$, there will be more water present. The values of these output parameters were determined for simulated periods of 1, 4 and 32 hours, all tested in the same fashion as benchmark 1D1 with adjusted continuity parameters.

The inputs of interest are the model parameters: θ_r, θ_s, ψ_a, n and K_s. The continuity parameters, S_s and ψ_0, were not included because they do not have a physical meaning. However, as said earlier, the model is very sensitive to these two parameters.

The ranges of the parameters are given in Table 3.1. They were chosen in conformity of their physical meaning (Bear, 1972) and according to the possible ranges in Hydrus 1D (Radcliffe and Šimůnek, 2010). For example, θ_r cannot be greater than θ_s in any case. Ranges for θ_s and θ_r were chosen as those used in Hydrus 1D. However, values below 0.38 for θ_s gave rise to convergence problems. The reason for this is probably that some combinations of input parameters along with values of θ_s below 0.38 do not work when used together with the continuity parameters. Similar problems occured when ψ_a was set at values lower than -3.5. According to Paniconi et al. (1991) n can be any value between 1.25 and 6 in benchmark setting 1D1. The bigger the n, the more m will approximate 1 and the MVG equations are gradually transformed into the Brooks & Corey model (Brooks and Corey, 1964; van Genuchten, 1980). However, it was observed that if n was greater than ± 3.25, that convergence problems aroused at the lower boundary. This is not a major issue because values of n greater than ± 3 are not much observed in field studies. The value of K_s has to be set lower than 0.0026 ms^{-1}. This can be derived from the convergence criterion Eq. (1.11):

$$\overline{K^t}_{i\pm1,j\pm1,k\pm1} \leq \frac{l^2 C^t_{i,j,k}}{\Delta t}, \tag{3.1}$$

with $\Delta t = 0.1$ s and $l = 0.1$ m. The lowest possible value for $C_{i,j,k}$ is S_s (Table 3.1) i.e. 0.026 m^{-1}. Recalling that K is $K_s \cdot K_r$, and the maximum of K_r is 1, one obtains from Eq. (3.1) that $K_s \leq 0.0026\ ms^{-1}$. Intuitively, the upper boundary constraint is a indirect example of the Courant–Friedrichs–Lewy (CFL) condition (Courant et al., 1928). The lower boundary for K_s was chosen to be $10^{-5}\ ms^{-1}$, which is classified under semi-pervious soil (Bear, 1972).

Table 3.1: Ranges of the soil hydraulic parameters considered in the GSA.

Input	θ_r	θ_s	Ψ_a	K_s	n
Units	[-]	[-]	[m]	[m s^{-1}]	[-]
Range	0.01 - 0.15	0.38 - 0.55	-0.1 - -3.5	10^{-5} - 0.0026	1.1 - 3.0

Finally, it has to be mentioned that some combinations of these parameters gave rise to convergence problems at the lower boundary near the GWT similar to the problem for a simulated period of 32 hours as seen in Figure 2.1. However, the problem

seemed to be contained in a small region near the GWT. Deviated values of ψ stabilized and they did not affect the greater upper part of the column, thus not affecting the output fitting parameters considerably.
The sampling design for this GSA is a Latin hypercube sampling (LHS). LHS is a statistical method for generating a near-random sample of parameter values from a multidimensional distribution. The sampling method is often used to construct computer experiments or for Monte-Carlo integration (Eglajs and Audze, 1977; McKay et al., 1979; Iman et al., 1981; Stein, 1987; Swiler and Wyss, 1987).
The model outputs were generated by running array job simulations on the high performance computer (HPC) of Ghent University (HPC @ UGent, 2018).
The estimator type was chosen to be variance-based. Variance-based methods have the capability to compute sensitivity indices regardless of the linearity of monotonicity, or other generic assumptions on the underlying model (Lilburne and Tarantola, 2009). In variance-based methods, the variance of the model outputs is decomposed into partial variances κ_i, which represent the share of κ that is explained by the model inputs:

$$\kappa = \sum_i \kappa_i + \sum_{i<j} \kappa_{ij} + \sum_{i<j<m} \kappa_{ijm} + \ldots + \kappa_{12\ldots k}, \tag{3.2}$$

with κ_i the share of the output variance explained by the ith model input, it represents the sensitivity of the model output Y to X_i; κ_{ij} is the share of the output variance explained by the interaction of the ith and jth inputs, it represents the sensitivity of Y to the interaction between X_i and X_j; k is the total number of model inputs. The first order sensitivity indices $S_i = \frac{\kappa_i}{\kappa}$ can be written in terms of conditional variances:

$$S_i = \frac{\kappa[E(Y \mid X_i)]}{\kappa(Y)}. \tag{3.3}$$

Method of Sobol'

The method of Sobol' provides appropriate formulae to estimate the terms in the decomposition of the output variance given in Eq. (3.2) (Sobol', 1993). The computational strategy for the Sobol' method works as follows:

- Choose an integer N as the sample size, here it was chosen to be 50.
- Generate a matrix $(N, 2k)$ of quasi-random rational numbers between 0 and 50 at intervals of 1. Split the matrix in two matrices of size (N, k), $k = 5$ (5 input parameters). From these matrices new matrices A and B are constructed so that

the ranges for the input parameters are all covered (Table 3.1). The columns of A and B are samples of the model inputs, extracted from their respective probability distributions.

- Define new matrices D_i formed by all columns of A, except the i_{th} column, which is taken from B, and a matrices C_i formed with the i_{th} column of A and with all the remaining columns of B.
- Compute the model output for all input values in matrices A, B, C_i and D_i, leading here to $2k+2=12$ vectors of model outputs of dimension N:

$$y_A = f(A), y_B = f(B), y_{C_i} = f(C_i), y_{D_i} = f(D_i). \tag{3.4}$$

The method of Sobol' estimates the first-order sensitivity indices as follows

$$\hat{S}_i = \frac{\hat{\kappa_i}}{\hat{\kappa}} = \frac{\hat{\kappa}_{X_i}[\hat{E_{X_{-i}}}(Y|X_i)]}{\hat{\kappa}} = \frac{y_A \cdot y_{C_i} - \hat{f}_0^2}{y_A \cdot y_A - \hat{f}_0^2} = \frac{\frac{1}{N}\sum_{j=1}^{N} y_A^{(j)} \cdot y_{C_i}^{(j)} - \hat{f}_0^2}{\frac{1}{N}\sum_{j=1}^{N}\left(y_A^{(j)}\right)^2 - \hat{f}_0^2}, \tag{3.5}$$

with the 'dot' indicating the scalar product between two vectors, $E_{X_{-i}}$ is the conditional expectation obtained by considering fixed values for X_i, and

$$\hat{f}_0^2 = \left(\frac{1}{N}\sum_{j=1}^{N} y_A^{(j)}\right)\left(\frac{1}{N}\sum_{j=1}^{N} y_B^{(j)}\right), \tag{3.6}$$

indicates the estimated average.

Thus, 3.5 becomes:

$$\hat{S}_i = \frac{\frac{1}{N}\sum_{j=1}^{N} y_A^{(j)} \cdot y_{C_i}^{(j)} - \left(\frac{1}{N}\sum_{j=1}^{N} y_{A_i}^{(j)}\right)\left(\frac{1}{N}\sum_{j=1}^{N} y_{B_i}^{(j)}\right)}{\frac{1}{N}\sum_{j=1}^{N} y_{A_i}^{(j)} \cdot y_{A_i}^{(j)} - \left(\frac{1}{N}\sum_{j=1}^{N} y_{A_i}^{(j)}\right)\left(\frac{1}{N}\sum_{j=1}^{N} y_{B_i}^{(j)}\right)}. \tag{3.7}$$

Vectors $y_A y_{C_i}$ and $y_B y_{D_i}$ are symmetrical, so another estimate for the first-order effect is

$$\hat{S}_i = \frac{\frac{1}{N}\sum_{j=1}^{N} y_B^{(j)} \cdot y_{D_i}^{(j)} - \left(\frac{1}{N}\sum_{j=1}^{N} y_{A_i}^{(j)}\right)\left(\frac{1}{N}\sum_{j=1}^{N} y_{B_i}^{(j)}\right)}{\frac{1}{N}\sum_{j=1}^{N} y_{B_i}^{(j)} \cdot y_{B_i}^{(j)} - \left(\frac{1}{N}\sum_{j=1}^{N} y_{A_i}^{(j)}\right)\left(\frac{1}{N}\sum_{j=1}^{N} y_{B_i}^{(j)}\right)}. \tag{3.8}$$

There are even more ways of computing $\hat{f}_0^2$ as shown in (Lilburne and Tarantola, 2009). Tarantola et al. (2006) proposed the following expression for $\hat{f}_0^2$

$$\hat{f}_0^2 = \left(\frac{1}{N}\sum_{j=1}^{N} y_{C_i}^{(j)}\right)\left(\frac{1}{N}\sum_{j=1}^{N} y_{D_i}^{(j)}\right), \tag{3.9}$$

thus, the first-order sensitivity indices can also be calculated as:

$$\hat{S}_i = \frac{\frac{1}{N}\sum_{j=1}^{N} y_A^{(j)} \cdot y_{C_i}^{(j)} - \left(\frac{1}{N}\sum_{j=1}^{N} y_{C_i}^{(j)}\right)\left(\frac{1}{N}\sum_{j=1}^{N} y_{D_i}^{(j)}\right)}{\frac{1}{N}\sum_{j=1}^{N} y_{C_i}^{(j)} \cdot y_{C_i}^{(j)} - \left(\frac{1}{N}\sum_{j=1}^{N} y_{C_i}^{(j)}\right)\left(\frac{1}{N}\sum_{j=1}^{N} y_{D_i}^{(j)}\right)}. \tag{3.10}$$

In total they developed 6 new estimates for the first order indices and propose to take the average of the 8 estimates to obtain one accurate mean for the first order indice (Lilburne and Tarantola, 2009).

The advantages and disadvantages using the Sobol' method are given in Table 3.2.

Table 3.2: Advantages and disadvantages of the Sobol' method

Advantages	**Disadvantages**
Model independent	Input parameters should be independent
Total-effect indices	Specific sampling strategy needed
High-order interactions	High computational demand
Using symmmetries makes this more efficient	
Can have spatial input that is auto-correlated	
Spatial structure included in SA	

Given its advantages, it becomes clear that the Sobol' method suits the GSA for this model. One clear example of a succesfully implemented integrated uncertainty- and SA using the Sobol' method can be consulted in Lingmann-Zielinska and Jankowski (2014).

3.1.3 Results & Discussion

Table 3.3 contains the results for a simulated period of 1 hour for each of the selected outputs: ψ_{MIN}, ψ_b and θ_{TOT}. Tables 3.4 and 3.5 contain the results for simulated periods of 4 hours and 32 hours, respectively. The first 8 rows are the estimates for the eight possible first-order sensitivity indices and the last row for the total effect indices.

The first thing to notice are negative indices. Negative Sobol' indices usually are not a problem, as long as they are close to zero, indicating that the input parameter has little first-order effect on the output parameter. This is not the case for most indices here, as they deviate a lot from zero. Secondly, the estimates of the indices frequently

deviate from each other (this will be discussed in more detail below). The values in each column should be more or less the same if the GSA is conducted succesfully. This is not the case, indicating a very low confidence level probably due to the low sampling size of $N = 50$. However, even given these serious remarks, there are some trends noticeable and not all of the above applies to each of the GSA runs.

Outputs for a simulated period of 1 hour

For ψ_{MIN}, the results do not make sense. Some first-order indices are greater than one and some go well below zero. The variance of ψ_{MIN} is not well predicted in terms of first-order effects given the defined variability of the input parameters. There are probably a lot of interactions among the input variables in the model (higher-order effects), which is most likely the reason given that the total effect indices also deviate from the first order indices.

Table 3.3: The 8 first-order sensitivity indices and the total effect indices for ψ_{MIN}, ψ_b and θ_{TOT} for a simulated period of **1 hour**.

Output	Indice	θ_r	θ_s	ψ_a	K_s	n
ψ_{MIN}	1.	-0.200145	0.367812	-0.049272	0.833407	-0.657558
	2.	0.014988	0.0686256	0.791066	0.247683	0.447848
	3.	0.101263	-0.186094	0.0249292	-0.421661	0.332691
	4.	0.0567569	-0.0146682	-2.31514	-0.445418	-0.258559
	5.	-0.101023	0.0473277	-2.02339	-0.919689	0.605201
	6.	-0.0296235	-0.135638	-1.56353	-0.489541	-0.885164
	7.	-0.0234663	0.327843	1.04874	1.36234	-0.12998
	8.	0.0417684	-1.0578	0.916576	2.81292	0.30424
	Total	-0.0671275	0.0880462	1.07488	0.346579	0.464472
ψ_b	1.	-0.0692926	-0.0562315	0.754778	0.0645271	-0.026049
	2.	-0.0968554	-0.0865865	0.719856	-0.0927927	0.0139339
	3.	-0.0862179	-0.0699665	0.93914	0.0802884	-0.032411
	4.	-0.102645	-0.0773098	0.891043	0.0335622	0.0647835
	5.	-0.0834876	-0.0636504	1.01289	0.0333544	0.043288
	6.	-0.0778418	-0.0695888	0.578542	-0.0745767	0.0111985
	7.	-0.113207	-0.0939079	0.702647	-0.122455	0.119031
	8.	-0.0920787	-0.0773159	0.798732	-0.121697	0.079536
	Total	-0.0021127	0.0107194	0.872968	0.091897	0.141504
θ_{TOT}	1.	0.0961004	-0.181253	0.251773	-0.0709903	0.391818
	2.	-0.0138516	0.0490092	0.282115	-0.0573623	0.304067
	3.	0.0812589	-0.153261	0.21289	-0.0600268	0.331307
	4.	0.0284266	0.0214702	0.243385	-0.0694525	0.519997
	5.	0.0358619	0.0169389	0.27784	-0.0818793	0.620673
	6.	-0.0163815	0.0579604	0.333641	-0.0678391	0.359603
	7.	-0.0704204	0.313271	0.316919	-0.0667961	0.488953
	8.	-0.0888395	0.247154	0.361783	-0.0787476	0.583619
	Total	0.106911	0.143222	0.384625	-0.0071318	0.63095

The variance of ψ_b after a simulated period of 1 hour is better explained in terms of first-order interactions. Here, the capillary air entry pressure ψ_a seems to play the most important role. Intuitively this seems logical, because this parameter is directly related to the effects that occur at the upper boundary where the soil is in contact with the atmosphere.

In case of output θ_{TOT}, the variance is more evenly attributed between the inputs. The pore-dimension distribution index, n, has a noticeable contribution to θ_{TOT} together with ψ_a. θ_r and θ_s have a small but significant contribution, K_s remarkably does not. Again, the first-order and total effect indices deviate from each other indicating higher-order effects.

Outputs for a simulated period of 4 hours

Again, the results for the output ψ_{MIN} do not make sense given the same reasons as mentioned above.

Table 3.4: The 8 first-order sensitivity indices and the total effect indices for ψ_{MIN}, ψ_b and θ_{TOT} for a simulated period of **4 hours**.

Output	Indice	θ_r	θ_s	ψ_a	K_s	n
ψ_{MIN}	1.	0.576901	0.38269	0.975519	-0.382896	1.76479
	2.	0.166727	0.172485	0.724049	0.268733	0.373146
	3.	0.155391	0.10308	0.262761	-0.103135	0.475356
	4.	0.163496	0.109408	-0.0528098	0.176538	0.168441
	5.	0.586595	0.274159	-0.0385242	0.188434	0.96116
	6.	0.618986	0.640363	2.68808	0.997689	1.38533
	7.	0.175347	0.18163	0.777495	0.68384	0.0802731
	8.	0.629115	0.455134	0.567174	0.729919	0.458055
	Total	0.071708	-0.140763	-0.410015	0.0931163	0.510385
ψ_b	1.	-0.0551197	-0.0876007	0.775456	0.1807	-0.0655377
	2.	-0.0627864	-0.0441353	0.562865	0.0347149	0.060648
	3.	-0.0444537	-0.0706493	0.6254	0.145734	-0.0528557
	4.	-0.0478371	-0.0613823	0.688123	0.179848	-0.0404609
	5.	-0.0616176	-0.0726875	0.805582	0.197628	-0.0344214
	6.	-0.0778512	-0.054725	0.697917	0.0430443	0.0751997
	7.	-0.0658841	-0.0339377	0.62148	0.0543393	0.0962549
	8.	-0.0848635	-0.0401883	0.727563	0.0597114	0.0818871
	Total	0.0097272	0.0024401	0.80529	0.214106	-0.0005735
θ_{TOT}	1.	0.101697	-0.187644	0.24855	-0.0686821	0.392542
	2.	-0.0138108	0.0487168	0.278106	-0.0534306	0.30836
	3.	0.0862766	-0.159192	0.210863	-0.0582679	0.333021
	4.	0.0308344	0.0269133	0.238638	-0.0715521	0.529146
	5.	0.0391472	0.0208259	0.273906	-0.0840173	0.624246
	6.	-0.0162792	0.0574239	0.327811	-0.0629802	0.363472
	7.	-0.0726359	0.329688	0.309765	-0.0667325	0.500903
	8.	-0.0922183	0.255117	0.355544	-0.078358	0.590926
	Total	0.107713	0.145075	0.380963	-0.0092651	0.633503

The variance of ψ_b for a simulated period of 4 hours is different compared to those of 1 hour. K_s seems to have gained importance, while n seems to have lost importance. Yet, ψ_a still is the most important one.

For the output parameter θ_{TOT} for a simulated period of 4 hours the results are quasi the same as for the 1 hour simulated period.

Outputs for a simulated period of 32 hours

The variance of ψ_{MIN} for a simulated period of 32 hours differs from those at 1 and 4 hours. ψ_a, K_s and n have a significant contribution of which ψ_a explains most variance. The reason for the difference with the two previous results may be attributed to the longer simulated period. Likely, many of the (50) runs had resulted in a quasi steady state condition.

For some combinations of input parameters, the values of output parameter ψ_b were greater than zero and had to be set to zero. Physically, $\psi_b > 0$ is not possible in the current setting.

The results for the output ψ_b are quasi the same as those for ψ_{MIN}. This is because ψ_b and ψ_{MIN} collide, as mentioned before. The lowest value ψ_{MIN} will, in many of the simulations, be located at the upper boundary.

The most important difference for the variance of θ_{TOT} after a simulated period of 32 hours compared to previous results is K_s. For simulated periods of 1 and 4 hours, K_s seems to play a minor role, while here it is the most important one. This is because K_s determines how fast the pressure head profile will shift and thus is directly related to the sum of water contents, θ_{TOT}.

GSA with a sample size of 200

A subsequent GSA with a sample size of N = 200 was carried out to obtain more accurate sensitivity indices. However, for each output only 2 of the 8 first order indices for ψ_a could be obtained. The other 6 of the first order indices together with the total effect indices were all obtained succesfully. The reason why only 2 indices were given for ψ_a is unknown.

For some simulated periods of 1, 4 and 32 hours, some values of ψ_b were greater than zero and had to be set to zero. For a sample size of 50 this only had to be done for a simulated period of 32 hours. But with N = 200, there are more input parameter combinations, and thus a higher probability that some of these combinations gave

Table 3.5: The 8 first-order sensitivity indices and the total effect indices for ψ_{MIN}, ψ_b and θ_{TOT} for a simulated period of **32 hours**.

Output	Indice	θ_r	θ_s	ψ_a	K_s	n
ψ_{MIN}	1.	-0.135759	-0.13596	0.407319	0.046903	0.211884
	2.	-0.161588	-0.161116	0.15764	0.175452	0.0221044
	3.	-0.161464	-0.161703	0.484441	0.0557841	0.252002
	4.	-0.161472	-0.162056	0.418192	0.14073	0.232618
	5.	-0.135741	-0.136098	0.576182	0.0753349	0.244076
	6.	-0.135863	-0.135467	0.132544	0.14752	0.0185854
	7.	-0.161596	-0.161469	0.142651	0.309062	0.0167454
	8.	-0.135845	-0.135605	0.196543	0.165446	0.0175702
	Total	-0.00004272	-0.0004227	0.573238	0.232754	0.358546
ψ_b	1.	-0.13556	-0.135639	0.405402	0.0461754	0.210816
	2.	-0.160992	-0.160843	0.156815	0.174237	0.0217523
	3.	-0.160925	-0.161019	0.481257	0.0548153	0.250262
	4.	-0.160921	-0.161018	0.417999	0.141598	0.231856
	5.	-0.135577	-0.135617	0.57496	0.0760624	0.243062
	6.	-0.135617	-0.135491	0.132098	0.146774	0.0183237
	7.	-0.160988	-0.160842	0.144265	0.309219	0.0167273
	8.	-0.135633	-0.135469	0.198437	0.166104	0.0175358
	Total	$4.0292*10^{-6}$	$-5.414*10^{-6}$	0.573642	0.233492	0.358924
θ_{TOT}	1.	0.00926508	-0.0790814	0.181538	0.342596	0.0924738
	2.	-0.154728	-0.0241813	0.338867	0.179961	-0.001329
	3.	0.0153888	-0.13135	0.301526	0.569034	0.153594
	4.	-0.11088	0.0571715	0.266556	0.264608	0.0996168
	6.	-0.0730887	0.0310325	0.171616	0.370295	0.0614548
	7.	-0.0931565	-0.0145587	0.20402	0.108348	-0.0008
	8.	-0.288642	0.17551	0.305824	0.0316864	-0.0772566
	9.	-0.190265	0.0952664	0.196898	0.0443422	-0.0476604
	Total	0.0423292	0.146257	0.351617	0.418232	0.189959

rise to model configurations that could generate convergence problems or physically impossible results ($\psi_b > 0$).

For a simulated period of 1 hour, the trends are quasi the same with again indications that ψ_{MIN} is a bad estimator for short simulated period or that even 200 runs are not enough to obtain reliable results.

The simulated period of 4 hours gives again unreliable results for ψ_{MIN}. The total effect indicices of ψ_b and θ_{TOT} are quasi the same as those of the GSA with N = 50.

For a simulated period of 32 hours there were major differences for ψ_b and slight differences for θ_{TOT}. Almost all variance of output parameter ψ_b can be attributed to K_s. For θ_{TOT}, θ_s's importance reduces to near zero.

However, it is hard to asses the relevance of the trends mentioned above, because these GSA results for N = 200 might not be reliable given the flaw for parameter ψ_a.

3.2 Validation

The constructed model was validated with field and experimental based parameters, obtained from Rezaei et al. (2017).

3.2.1 Field and experimental data

In Rezaei et al. (2017) a quasi 3D modelling approach was developed by integrating a crop growth (LINGRA-N) and hydrological model (Hydrus-1D) (Radcliffe and Šimůnek, 2010) to simulate and visualize water flow, soil-water storage, water stress and crop yield over a heterogeneous sandy field. The computational efficiency and uncertainty with low- to high-spatial resolation input factors (soil-hydraulic properties, soil-layer thickness and GWT level) and evaluated irrigation scenarios to find the optimal and cost-effective irrigation scheduling.

The study site is located in an agricultural area at the border between Belgium and the Netherlands (with central coordinates 51°19’05" N, 05°10’40" E, Figure 3.1), characterized by a temperate maritime climate with mild winters and cool summers. During the study period 2011-2013, the farmer cultivated grass. The 10.5 ha field is almost flat (less than 1 % sloping up from the North-West to the South-East) and runoff is not considered to be important. The major soil is typical Podzol (Zcg-Zbg type moderately drained sandy soils with a clear horizont according to the Belgian soil classification) or Albic Podzols (Arenic) according to WRB (FAO, 2014) with distinct Ap and C horizons. Maximum grass root density was found at about 6 cm and decreased from 6 cm to the bottom of the Ap horizon (based on field observations). Based on observations, it was concluded that the depth of the GWT varied from 70 to 155 cm, and the Ap horizon thickness was between 30 and 50 cm at various locations across the field depending on the topography. The field is partly drained by parallel drainage pipes, connected to a ditch at the North-West border. They are placed at 10-20 cm intervals and at about 90 cm below the soil surface. Some assumptions were necessary for the quasi 3D modelling of water flow in the vadose zone: 1) only vertical flow was considered; 2) the upper boundary conditions are uniform for all locations over the field; and 3) a constant head bottom boundary condition was assumed (with specified depth of groundwater for each location). The latter is justified for the field study site given the presence of the drainage system.

To determine the hydraulic conductivity K_s and SWRC, $\theta(h)$, two undisturbed soil samples were taken within a radius of maximum 20 cm with cores of 5 cm diameter and 5 cm height (100 cm^3 Kopecky rings, Eijkelkamp Agrisearch Equipment, Geisbeek, the

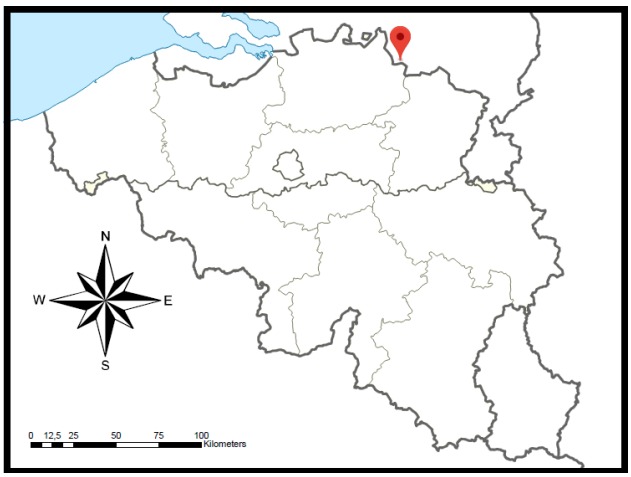

Figure 3.1: Location of the agricultural field of study at the Belgium-Netherlands border

Netherlands) at a depth of 20 cm within the Ap horizon (topsoil) and 70 cm within the C horizon (subsoil) at 28 locations. K_s was determined using a constant head labratory permeameter (M1-0902e, Eijkelkamp Agrisearch Equipment). The SWRC, $\theta(h)$ was determined using the sandbox method (Eijkelkamp Agrisearch Equipment) up to a matric head of -100 cm and the standard pressure plate apparatus (Soilmoisture Equipment, Santa Barbara CA, USA) for matric heads equal to or below -200 cm. Table 3.12 contains the averages and ranges of the fitted characteristic curves (Rezaei et al., 2017).

Table 3.6: Average and range of soil hydraulic properties of the two layers of the entire field of study. The coefficient of variation, CV is expressed in percentage.

		K_s **[cm h^{-1}]**	θ_r **[-]**	θ_s **[-]**	α **[cm^{-1}]**	n **[-]**
Topsoil (Ap)	Average	3.94	0.08	0.39	0.17	2.05
	Range	0.61-13.8	0.01-0.11	0.35-0.47	0.012-0.038	1.27-3.53
	CV	78.0	20.9	5.3	39.3	22.8
Subsoil (C)	Average	2.27	0.05	0.32	0.020	2.52
	Range	0.4-7.9	0.02-0.12	0.29-0.40	0.01-0.04	1.51-3.22
	CV	59.3	59.6	11.94	40.62	2768

In this study it was shown that changes in soil-water content are most sensitive to K_s. It was also found that calibrating the model by optimizing K_s and keeping all other MVG hydraulic parameters constant should suffice for irrigation management purposes.

3.2.2 Data for validation

Table 3.7 gives 9 hydraulic parameter sets that were provided from Rezaei et al. (2017) to compare results between the simulations with the CML model and Hydrus-1D. An infiltration- and evaporation scenario was chosen to be applied to all of these parameter sets. This scenario covered a simulated period of 30 days in which 35 mm precipitation falls in the first ten days; then there is evaporation of half this amount of water in the following 10 days, to finish with again an infiltration of 70 mm in the last 10 days. The initial state is a hydrostatic equilibrium ($\psi + z = 0$). All of the fluxes were implemented uniformly both in the CML model and Hydrus-1D. Hysteresis and root water uptake were not considered.

Table 3.7: Nine hydraulic parameter sets provided for the validation.

ID	**layer [cm]**	θ_r **[cm^3 cm^{-3}]**	θ_s **[cm^3 cm^{-3}]**	α **[cm^{-1}]**	n **[-]**	K_s **[cm h^{-1}]**
1.	Topsoil (0 - 34)	0.107	0.422	0.018	2.784	9.594
	Subsoil (35 - 140)	0.026	0.305	0.021	2.341	4.730
2.	Topsoil (0 - 40)	0.084	0.355	0.013	2.019	2.106
	Subsoil (41 - 112)	0.046	0.315	0.014	3.338	1.618
3.	Topsoil (0 - 39)	0.098	0.359	0.013	2.050	3.776
	Subsoil (40 - 120)	0.068	0.406	0.026	1.668	4.026
4.	Topsoil (0 - 39)	0.091	0.362	0.015	2.647	4.370
	Subsoil (40 - 122)	0.044	0.318	0.016	2.426	1.424
5.	Topsoil (0 - 40)	0.059	0.402	0.027	1.957	3.406
	Subsoil (41 - 113)	0.031	0.304	0.017	2.911	1.454
6.	Topsoil (0 - 43)	0.088	0.381	0.014	3.095	2.515
	Subsoil (44 - 92)	0.015	0.285	0.019	3.076	1.586
7.	Topsoil (0 - 45)	0.083	0.340	0.011	1.968	0.777
	Subsoil (46 - 76)	0.060	0.374	0.383	1.484	2.200
8.	Topsoil (0 - 43)	0.089	0.341	0.008	2.223	0.822
	Subsoil (44 - 80)	0.120	0.392	0.005	2.642	0.399
9.	Topsoil (0 - 40)	0.063	0.372	0.015	3.795	2.809
	Subsoil (41 - 94)	0.052	0.621	0.019	2.750	5.390

Preliminary simulations in Hydrus 1D showed interesting profiles for parameter sets 1, 5 and 7. Due to time constraints, as a consequence of the long computation times of the CML model, only these 3 sets were considered for simulations with the CML model. Moreover, runs with Hydrus on parameter sets 2, 3, 4, 6, 8 and 9 showed similar results as parameter sets 1 and 5.

3.2.3 Results & Discussion

In the following section each pressure head profile obtained with the CML model is compared to its counterpart obtained with Hydrus. For the sake of clarity and to not overburden the graphs, the pressure head profiles for the simulated periods of 25 and 30 days were not included, but discussed in the text.

Validation parameter set 1

As can be seen in Figures 3.2 and 3.3, there are two main differences in the simulations between Hydrus and the CML model.

1. The pressure head profiles at day 10, 20 and 30 are more shifted to the left (for evaporation) for the CML model.
2. The pressure head profiles at day 5, 15 and 25 of the CML model lag behind compared to those of the Hydrus simulations.

Indeed, in Figure 3.2 the pressure head profile at 20 days is shifted to the left compared to the profile at the same simulated time obtained with Hydrus. Item 2 is a bit harder to see on these figures. In Figure 3.2, at a simulated time of 5 days, the profile in red has not yet reached the state at day 10. On the contrary, in Figure 3.3 this is the case, as the pressure head profile at 5 days and 10 days collide.

The slower convergence of the CML model is due to significant lower hydraulic conductivity values which on their turn are probably related to differences in the model structures and in the way the MVG equations are used. Indeed, the MVG equation for the CML were modified versions of the original MVG equations, but the observed differences can not be justified by these modifications. Another important factor concerns the continuity parameters, ψ_0 and S_s, which are not present in Hydrus model structure and thus might be the cause of this lagging.

Validation parameter set 5

For parameter set 5 the problems are similar, the shift to the left of the pressure head profile is even more marked now (compare pressure head profiles at 20 days in Figure 3.4 and 3.5).

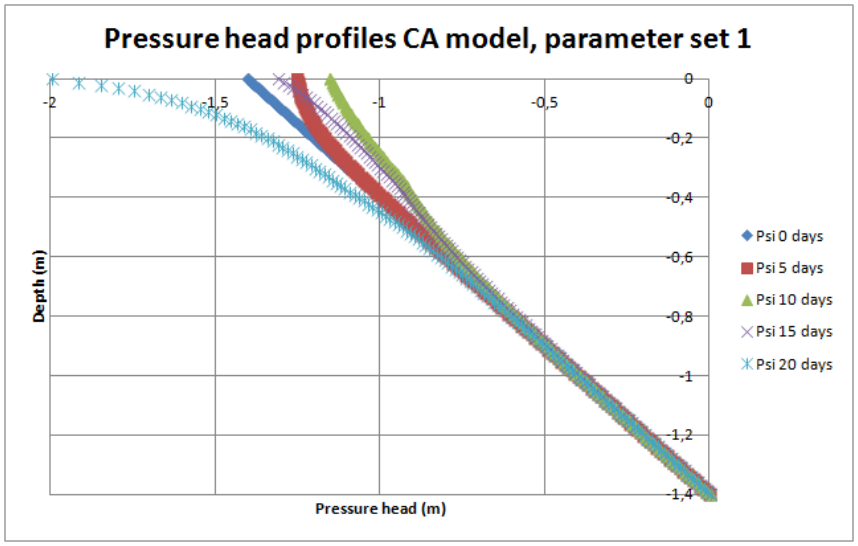

Figure 3.2: Pressure head profiles for parameter set 1 at simulated times of 0, 5, 10, 15, 20, 25 and 30 days for the CML model

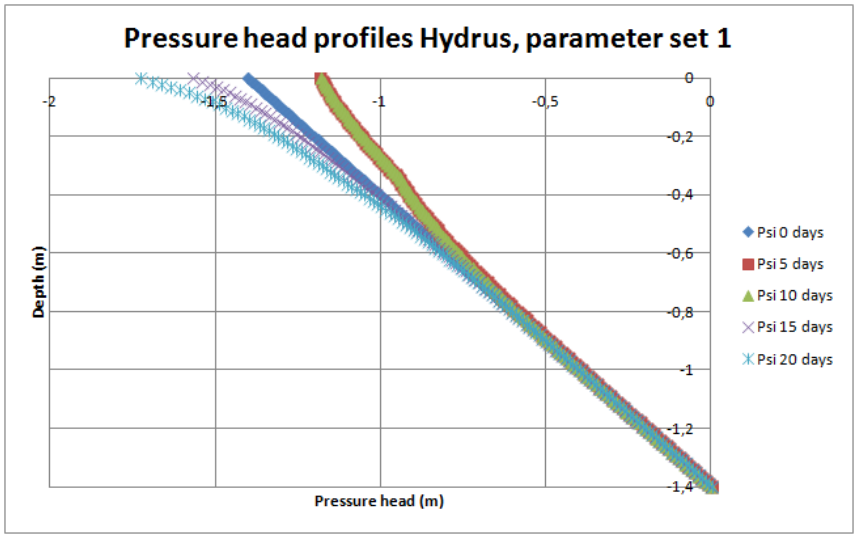

Figure 3.3: Pressure head profiles for parameter set 1 at simulated times of 0, 5, 10, 15, 20, 25 and 30 days in Hydrus

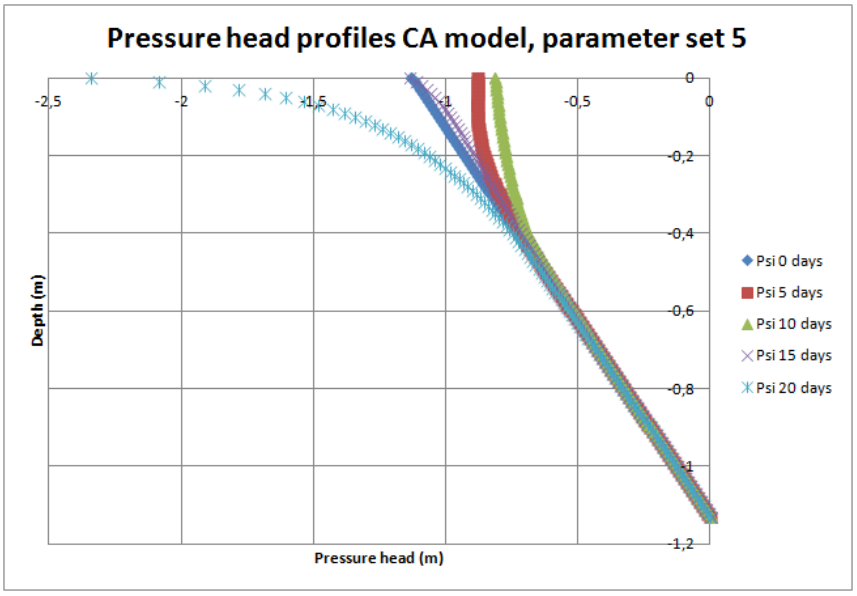

Figure 3.4: Pressure head profiles for parameter set 5 at simulated times of 0, 5, 10, 15, 20, 25 and 30 days for the CML model

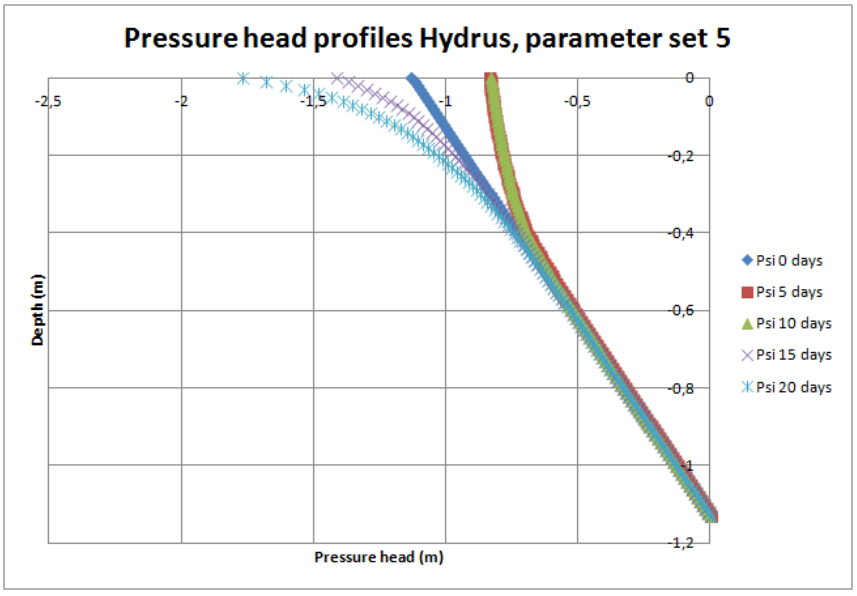

Figure 3.5: Pressure head profiles for parameter set 5 at simulated times of 0, 5, 10, 15, 20, 25 and 30 days in Hydrus

Validation parameter set 7

Parameter set 7 is different from set 1 and 5. The presence of the second layer can now cleary be seen (Figure 3.6 and 3.7). The kink in the curves mark the separation of the two layers at a depth of 43 cm under the surface. The reason for this different behaviour is the high inverse air entry pressure value (α) of the second layer (Table 3.13). Another difference with the previous parameter sets is the low K_{sat} value in the first layer.

The problems are again similar, the shift is even more marked here as can be seen for a simulated period of 20 days.

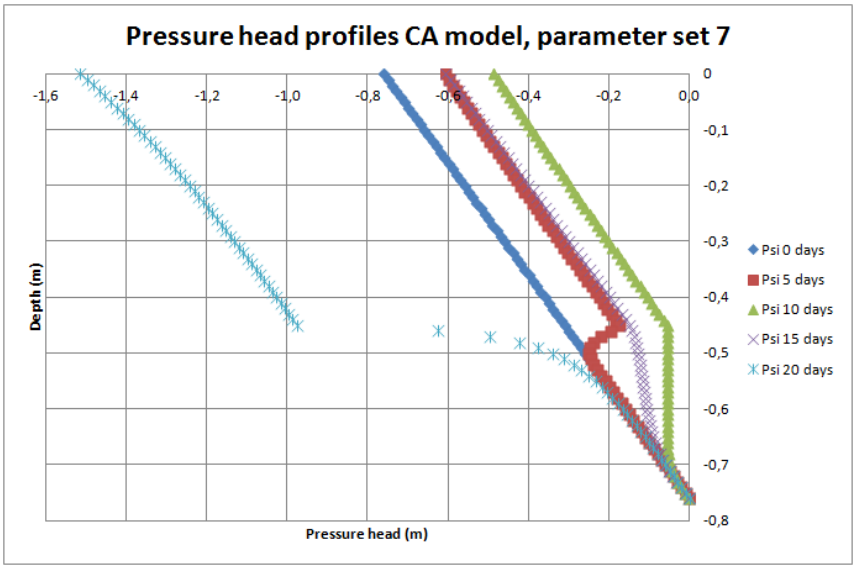

Figure 3.6: Pressure head profiles for parameter set 7 at simulated times of 0, 5, 10, 15, 20, 25 and 30 days for the CML model

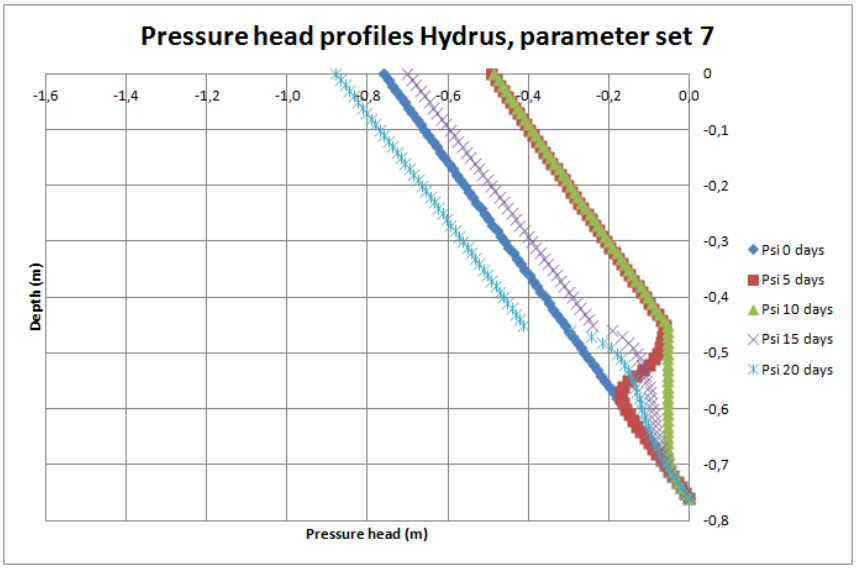

Figure 3.7: Pressure head profiles for parameter set 7 at simulated times of 0, 5, 10, 15, 20, 25 and 30 days in Hydrus

The accuracy of the CML with respect to Hydrus 1D was estimated using the mean squared error (MSE):

$$MSE(t) = \sum_{i=1}^{n} \frac{\left[\psi_{CML}(z_i, t) - \psi_{Hydrus}(z_i, t)\right]^2}{n}, \tag{3.11}$$

with ψ_{CML} and ψ_{Hydrus} the pressure heads in cell z_i and time t for the CML- and Hydrus simulations respectively. The results, given in Table 3.8, confirm the trends observed earlier.

Table 3.8: MSE terms for parameter sets 1, 5 and 7.

	Simulated period, in days					
MSE, in m^2	**5**	**10**	**15**	**20**	**25**	**30**
1.	0,003059	0,000095	0,008850	0,002118	0,022100	0,000049
5.	0,001154	0,000012	0,005057	0,007143	0,036795	0,000039
7.	0,010704	0,000001	0,005503	0,210520	0,475372	0,000001

CHAPTER 4

MODEL MODIFICATION

To circumvent the use of the convergence parameters S_s and ψ_0, an attempt was made to modify the CML model. Instead of using the modified MVG equations by van Genuchten and Nielsen (1985) described in Paniconi et al. (1991), the use of the continuity parameters was omitted. For θ and K, Eqs. (1.36), (1.37) were used and the water retention capacity becomes:

$$C_w(\psi) = \begin{cases} (-m)(\theta_s - \theta_r)\left[1 + \left(\frac{\psi}{\psi_a}\right)^n\right]^{-m-1} n\left(\frac{\psi}{\psi_a}\right)^{n-1}\left(\frac{1}{\psi_a}\right), & \psi < 0, \\ 0, & \psi \geq 0. \end{cases} \tag{4.1}$$

When running this updated CML model for benchmark 1D1 with a spatial discretization of 1 cm, thus 101 cells, the convergence problems occured immediately. A way to solve this problem was to increase the spatial discretization. Indeed, when using 41, 31 or 21 cells, the convergence problem did not occur. The computing time also descreased quasi linearly with respect to the amount of cells used. The main drawback is a lower resolution of the obtained simulated pressure head profile.

CHAPTER 5

CONCLUSION AND DISCUSSION

In Chapter 2 it became clear that there were some major issues with the CML model. The values of the continuity parameters S_s and ψ_0 in benchmark 1D1, which guarantee the convergence of the simulation, had to be adjusted in comparison to the original values used in CAMElot. If not, the model did not converge even for short simulation periods. The adjustment of these parameters was done manually and the model showed better results except for simulation times around 30 hours, when the convergence problem occured at the bottom of the column. The continuity parameters in benchmark 1D2 had to be adjusted as well, but this benchmark setting did not lead to convergence problems at higher simulation times. Even though S_s and ψ_0 have no real physical meaning and were implemented because out of necessity (Paniconi et al., 1991), it is odd that they had to be adjusted in comparison to the simulations in CAMElot in which they seemingly posed no troubles. In the two dimensional benchmark, the continuity parameter S_s caused major problems. The original value of S_s, i.e. 0, this is not possible because of division by 0 errors in the model equations. S_s was adjusted gradually to 0.6 to obtain runs that did converge. However, this time the steady state result at 5 days of simulated time did not match the original result, indicating that S_s had a significant undesired influence on the simulation. The structure of the CML seems to work, but only the used physical equations tend to give rise to the problems.

The convergence problems are directly related to the convergence criterion (Eq. 2.3) and possible local violations of the CFL condition when the criterion is not fulfilled (Courant et al., 1928). This restriction increases the computational burden dramatically when large scale problems are examined with unfavourable soil hydraulic properties and boundary conditions (Anagnostopoulos and Burlando, 2012). Anagnostopoulos and Burlando (2012) propose a way to solve the problem by modifying the model to an unconditonally stable structure and implementing an iteration scheme. In a sense, one does not have a CML anymore, it is combined with iteration methods. This is a set back for the CML philosphy, because they were developed for the very reason to avoid complicated discretisation and iteration schemes.

In Chapter 3 we conclude a significant contribution to variance from input parameters ψ_a, K_s and n for their given ranges. Overall, ψ_a has the most prominent contribution. θ_r and θ_s have a very low contribution, which is in agreement with Rezaei et al. (2017). In preparation of the GSA, namely setting up the ranges of the input parameters and testing them preliminary, two other problems were noticed. First, n had to be kept at a value lower than approximately 3.0 and θ_s had to be chosen higher than approximately 0.38. If not, convergence problems arose in combination with the other input parameters in their ranges and the fixed continuity parameters. However, these boundaries were not absolute, meaning that in most seperate runs they will not pose problems if the continuity parameters are adjusted. This is due to the non-linear behaviour of the MVG equations.

This complex non-linear behaviour may require more samples to a achieve a higher accuracy for the sensitivity estimates. It is possible that a sample size of 200 was still not sufficient to obtain accurate indices. However, some trends were already clear in the GSA with a sample size of 50. In addition, the results of the GSA with a sample size of 200 were not reliable given the flaws for input parameter ψ_a. It would be interesting to asses a GSA for benchmark 1D2 and compare the results with the GSA for the 1D1 benchmark. The outputs ψ_b and θ_{TOTAL} could be compared, but ψ_{MIN} has no equivalent in the 1D2 benchmark since it is the same as ψ_b. A new output that could be assesed is the inflection point of the pressure head profiles (see Figure 2.2). Due to time constraints this GSA could not be conducted.

For what concerns the validation, it was shown that the CML model performance was low compared to the Hydrus 1D software. The discretization and iteration schemes of Hydrus are efficient and flexible and so the computing time is next to nothing. Although the structure of the CML model lends itself to parallelization, it can not live up to the goals it was created for. A way to lower the computing time is to compile the mathematica source code to C or another program language (CCodeGenerator, 2018). In this way, the computing time could be lowered with a factor of 10 to 30. In addition the quantization method of Zeigler (1998) as implemented in Mendicino et al. (2006) would help to reduce it even further.

BIBLIOGRAPHY

Ahrens, C. D. (2000). *Meteorology today: An introduction to weather, climate, and the environment*. Pacific Grove, CA: Brooks/Cole Pub.

Anagnostopoulos, G. G. and Burlando, P. (2012). An Object-oriented computational framework for the simulation of variably saturated flow in soils, using a reduced complexity model. *Environmental Modelling & Software*, 38:191–202.

Baetens, J. and Nopens, I. (2016). *Modelling and simulation 2*. Faculteit Bio-ingenieurswetenschappen, Universiteit Gent.

Bear, J. (1972). Dynamics of Fluids in Porous Media. *American Elsevier Publishing Company, New York*.

Berec, L. (2002). Techniques of spatially explicit individual-based models: construction, simulation and mean-field analysis. *Ecological Modelling*, 150:55–81.

Botula, Y.-D., Nemes, A., Mafuka, P., Van Ranst, E., and Cornelis, W. M. (2013). Prediction of water retention of soils from the humid tropics by the nonparametric-nearest neighbor approach. *Vadose Zone Journal*, 12.

Brooks, R. and Corey, A. (1964). Hydraulic properties of porous media. *Hydrology Paper 3, Calorado State Univ., Fort Collins, CO.*

Buckingham, E. (1907). *Studies on the movement of soil moisture*, volume Bull. No. 38. U.S. Department of Agriculture.

Burrough, P. A. and McDonnel, R. (1998). Principles of Geographic Information Systems. *Oxford University Press*.

CCodeGenerator (2018). Wolfram mathematica, documentation center. http://reference.wolfram.com/language/CCodeGenerator/guide/CCodeGenerator.html.

Cervarolo, G., Mendicino, G., and Senatore, A. (2011). Coupled vegetation and soil moisture dynamics modeling in heterogeneous and sloping terrains. *Vadose Zone Journal*, 10:206–225.

Cornelis, W. M., Kloshi, M., Hartmann, R., Van Meirvenne, M., and Vos, B. D. (2005). Comparison of unimodal analytical expressions for the soil-water retention curve. *Soil Science Society of America Journal*, 69:1902–1911.

Cosmi, F. (2004). Two-dimension estimate of effective properties of solid with random voids. *Theoretical and applied fracture mechanics*, 42(2):183–189.

Cosmi, F. (2005). Elastodynamics with the cell method. *Computer Modeling in Engineering & Sciences*, 8(3):191–200.

Courant, R., Friedrichs, K., and Lewy, H. (1928). Über die partiellen Differenzengleichungen der mathematischen Physik. *Mathematische Annalen*, 100(1):32–74.

Cusatis, G., Rezakhani, R., and Schauffert, E. (2017). Discontinuous Cell Method (DCM) for the simulation of cohesive fracture and fragmentation of continuous media. *Engineerign fracture mechanics*, 170:1–22.

Darcy, H. (1856). Les fontaines publiques de la ville de Dijon. *Paris: Dalmont*.

Dattilo, G. and Spezzano, G. (2003). Simulation of a cellular landslide model with CAMELOT on high performance computers. *Parallel Computing*, 29(10):1403–1418.

Eglajs, E. and Audze, P. (1977). New approach to the design of multifactor experiments. *Problems of dynamics and strengths. Riga: Zinatne Publishing House*, 35:104–107.

FAO (2014). World Reference Base for Soil Resources 2014. *World Soil Recourses Reports, FAO, Rome, Italy*, page 191.

Ferretti, E. (2003). Crack propagation modeling by remeshing using the cell method (CM). *Computer Modeling in Engineering & Sciences*, 4(1):51–72.

Ferretti, E., Casadio, E., and Leo, A. D. (2003). Masonry walls under shear test: a CM modeling. *Computer Modeling in Engineering & Sciences*, 30(3):163–189.

Folino, G., Mendicino, G., Senatore, A., Spezzano, G., and Salvatore, S. (2006). A model based on cellular automata for the parallel simulation of 3D unsaturated flow. *Parallel Computing*, 32:357–376.

Fonstad, M. (2006). Cellular automata as analysis and synthesis engines at the geomorphology-ecology interface. *Geomporhology Elsevier*, 77:217–234.

Fürst, T., Vodák, R., Šír, M., and Bíl, M. (2009). On the incompatibility of Richards' equation and finger-like infiltration in unsaturated homogeneous porous media. *Water Resources Research*, 45(WR03408):12.

Gardner, M. (1995). The fantastic combinations of John Conway's new solitary game of "Life". *Scientific American*, 223:120–123.

Gerke, H. and van Genuchten, M. T. (1993). A dual-porosity model for simulating the preferential movement of water and solutes in structured porous-media. *Water Resources Research*, 29(2):305–319.

Germann, P. (2010). Comment on "Theory for source-responsive and free-surface film modeling of unsaturated flow". *Vadose Zone Journal*, 9(4):1000–1101.

Glass, R. J. and Yarrington, L. (2003). Mechanistic modeling of fingering, nonmonotonicity, fragmentation, and pulsation within gravity/buoyant destabilized two-phase/unsaturated flow. *Water Resources Research*, 39(3):1058.

Gray, W. G. and Hassanizadeh, S. (1991). Paradoxes and realities in unsaturated flow theory. *Water Resources Research*, 27(8):1847–1854.

Gurikov, P., Kolnoochenko, A., Golubchikov, M., Menshutina, N., and Smirnova, I. (2016). A synchronous cellular automaton model of mass transport in porous media. *Computers and Chemical Engineering*, 84:446–457.

HPC @ UGent (2018). High performance computing infrastructure, Ghent University. https://www.ugent.be/hpc/en.

Huang, K., Mohanty, B. P., and van Genuchten, M. (1996). A new convergence criterion for the modified Picard iteration method to sole the variably saturated flow equation. *Journal of Hydrology*, 178:69–91.

Huyakorn, P. S., Thomas, S. D., and Thompson, B. (1984). Techniques for making tfinite elements competitive in modeling flow in variably saturated porous media. *Water Resources Research*, 20(8):1099–1115.

Iman, R., Helton, J., and Campbell, J. (1981). An approach to sensitivity analysis of computer models, Part 1. Introduction, input variable selection and preliminary variable assessment. *Journal of Quality Technology*, 13(3):174–183.

Indelman, P. and Dagan, G. (1993). Upscaling of permeability of anisotropic heterogeous formations: 1. The general framework. *Water Resources Research*, 29(4):917–923.

Ippisch, O., Vogel, H. J., and Bastian, P. (2006). Validity limits for the van Genuchten-Mualem model and implications for parameter estimation and numerical simulation. *Advances in Water Resources*, 29:1780–1789.

Jarvis, N. and Larsbo, M. (2012). MACRO (v5.2): Model use, calibration, and validation. *Transaction of the Abase*, 55(4):1413–1423.

Knabner, P. and Angermann, L. (2003). Numerical methods for elliptic and parabolic partial differential equations. *Springer*.

Lilburne, L. and Tarantola, S. (2009). Sensitivity analysis of spatial models. *International Journal of Geographical Information Science*, 23(2):151–168.

Lingmann-Zielinska, A. and Jankowski, P. (2014). Spatially-explicit integrated uncertainty and sensitivity analysis of criteria weights in multicriteria land suitability evaluation. *Environmental Modelling & Software*, 57:235–247.

List, F. and Radu, F. A. (2016). A study on iterative methods for solving Richards' equation. *Comput. Geosci.*, 20:341–353.

Margolus, N., Toffoli, T., and Vichniac, G. (1986). Cellular-Automata Supercomputers for Fluid-Dynamics Modeling. *Laboratory for Computer Science, MIT*, 56(16).

McDonald, M. and Harbaugh, A. (1988). A modular three-dimensional finite-difference ground-water flow model. *Techniques of Water-Resources Investigations, U.S. Geological Survey*, 6(16).

McKay, M., Beckman, R., and Conover, W. (1979). A Comparison of three Methods for selecting values of input variables in the analysis of output from a computer code. *Technometrics (JSTOR Abstract). American Statistical Association.*, 21(2):239–245.

Mendicino, G., Senatore, A., Spezzano, G., and Straface, S. (2006). Three-dimensional unsaturated flow modeling using cellular automata. *Water Resources Research*, 42:W11419, doi:10.1029.

Mualem, Y. (1976). A new model for predicting the hydraulic conductivity of unsaturated porous media. *Water Resources Research*, 12:513–522.

Nopens, I. (2015). *Modelleren en simuleren van biosystemen*. Faculteit Bioingenieurswetenschappen, Universiteit Gent.

Paniconi, C., Aldama, A. A., and Wood, E. F. (1991). Numerical evaluation of iterative and noniterative methods for the solution of the nonlinear Richards equation. *Water Resources Research*, 27(6):1147–1163.

Paniconi, C. and Putti, M. (1994). A comparison of Picard and Newton iteration in the numerical solution of multidimensional variably saturated flow problems. *Water Resources Research*, 30(12):3357–3374.

Paniconi, C. and Putti, M. (2015). Physically based modeling in catchment hydrology at 50: Survey and outlook. *Water Resources Research*, 51:7090–7129, doi:10.1002.

Radcliffe, D. and Šimůnek, J. (2010). *Soil Physics with HYDRUS: modeling and applications*. CRC Press Boca Raton, Florida.

Ravazzani, G., Rametta, D., and Mancini, M. (2011). Macroscopic cellular automata for groundwater modelling: A first approach. *Environmental Modelling & Software*, 26:634–643.

Rezaei, M., De Pue, J., Seuntjes, P., Joris, I., and Cornelis, W. (2017). Quasi 3D modelling of vadose zone soil-water flow for optimizing irrigation strategies: Challenges, uncertainties and efficiencies. *Environmental Modelling & Software*, 93:59–77.

Richards, L. A. (1931). Capillary conduction of liquids through porous mediums. *Environmental Modelling & Software*, 1(5):318—-333.

Richardson, L. F. (1922). Weather prediction by numerical process. *Cambridge, The University press*, 1(5):262.

Saltelli, A., Ratto, M., Andres, T., Campolongo, F., abd J., C., Gatelli, D., Saisana, M., and Tarantola, S. (2008). Global Sensitivity Analysis. The Primer. *John Wiley & Sons, Ltd*.

Schaap, M. G. and van Genuchten, M. (2005). A modified Mualem-van Genuchten formulation for Improved description of the hydraulic conductivity near saturation. *Vadose Zone Journal*, 5:27–34.

Short, D., W.R., D., and White, I. (1995). The practicability of using Richards' equation for general purpose soil-water dynamics models. *Environmental International*, 21(5):723–730.

Shukla, M. K. (2014). *Soil Physics: An Introduction*. CRC Press, Taylor and Francis group.

Sobol', I. M. (1993). Sensitivity estimates for nonlinear mathematical models. *Modeling and Computational Experiment*, 1:407–414.

Stein, M. (1987). Large sampling properties of simulations using Latin Hypercube Sampling. *Technometrics*, 29(2):143–151.

Swiler, L. and Wyss, G. (1987). A User's guide to Sandia's Latin Hypercube Sampling Software: LHS UNIX Library/Standalone version. *United States: N. p.*, pages 143–151.

Szymkiewicz, A. (2009). Approximation of internodal conductivities in numerical simulation of one-dimensional infiltration, drainage, and capillary rise in unsaturated soils. *Water Resources Research*, 45:1–16.

Tarantola, S., Nardo, M., Saisana, M., and Gatelli, D. (2006). A new estimator for sensitivity analysis of model output: an application to the e-business readiness composite indicator. *Reliability Engineering and System Safety*, 91:1135–1141.

Theis, C. (1935). The relation between the lowering of the piezometric surface and the rate and duration of discharge of a well using groundwater storage. *Transactions of The American Geophyical Union*, 16:519–524.

Tobler, W. (1979). Cellular geography. *In: Gale, S., Olsson, G. (Eds.), Philosophy in Geography. D. Reidel, Dordrecht, The Netherlands*, pages 279–386.

Tocci, M. D., Kelley, C. T., and Miller, C. (1997). Accurate and economical solution of the pressure-head form of Richards' equation by the method of lines. *Water Resources Research*, 20(1):1–14.

Toffoli, T. and Margolus, N. (1987). Cellular Automata Machines. *MIT Press, Cambridge, MA*, page 259.

Tonti, E. (2001). A discrete formulation of field laws: The cell method. *Computer Modeling in Engineering & Sciences*, 1(1):11.

Tonti, E. (2002). Finite formulation of electromagnetic field. *IEEE Transactions on Magnetics*, 38(2):333–336.

Tonti, E. and Zarantonello, F. (2010). Algebraic Formulation of Elastodynamics: the Cell Method. *Computer Modeling in Engineering & Sciences*, 64(1):37–70.

USGS Water Science School (2017a). The Vadose Zone - USGS Water Science School. (source:https://water.usgs.gov/ogw/unsaturated.html).

USGS Water Science School (2017b). The Water Cycle - USGS Water Science School. https://water.usgs.gov/edu/watercycle.html.

van Dam, J. C., Stricker, J. N. M., and Drooger, P. (1994). Inverse method to determine soil hydraulic function from multistep outflow experiments. *Soil Science Society of America Journal*, 58:647–652.

van Genuchten, M. T. (1980). A closed-form equation for predicting the hydraulic conductivity of unsaturated soils. *Soil Science Society of America Journal*, 44:892–898.

van Genuchten, M. T. and Nielsen, D. R. (1985). On describing and predicting the hydraulic properties of unsaturated soils. *Ann. Geophys.*, 3(5):615–628.

Vereecken, H., Weynants, M., Javaux, M., Pachepsky, Y., Schaap, M. G., van Genuchten, M. T., and Others (2010). Using pedotransfer functions to estimate the van Genuchten-Mualem soil hydraulix properties: A review. *Vadose Zone Journal*, 9:795–820.

Viola, E., Tornabene, F., Ferretti, E., and Fantuzzi, N. (2013). Soft core plane state structures under static loads using GDQFEM and cell method. *Computer Modeling in Engineering & Sciences*, 94(4):309–329.

Vogel, T., van Genuchten, M. T., and Cislerova, M. (2001). Effect of the shape of the soil hydraulic functions near saturation on variably-saturated flow predictions. *Advances in Water Resources*, 24:133–144.

von Neumann, J. (1966). Theory of Self-Reproducing Automata. *Urbana, University of Illinois Press*.

Wolfram, S. (1986). Theory and Application of Cellular Automata. *World Scientific Publishing, Singapore*.

Wolfram, S. (1994). Cellular Automata and Complexity. *Addison-Wesley, Boston, Mass*.

Wolfram Mathematica (2018). Wolfram mathematica: Modern technical computing. https://www.wolfram.com/mathematica/.

World Population Clock (2017). The world population clock: 7.6 billion people (2018). http://www.worldometers.info/world-population/.

Zeigler, B. P. (1998). DEVS theory of quantized systems. *Advanced Simulation Technology Thrust DARPA contract N6133997K-0007, Department of Electrical and Computer Engineering University of Arizona, Tucson, Arizona*.